Monthly Notices
of the
ROYAL ASTRONOMICAL SOCIETY

Mon. Not. R. Astron. Soc. **410,** 2057–2074 (2011) doi:10.1111/j.1365-2966.2010.17583.x

Polarization as an indicator of intrinsic alignment in radio weak lensing

Michael L. Brown[1,2⋆] and Richard A. Battye[3⋆]

[1]*Astrophysics Group, Cavendish Laboratory, University of Cambridge, J. J. Thomson Avenue, Cambridge CB3 OHE*
[2]*Kavli Institute for Cosmology, University of Cambridge, Madingley Road, Cambridge CB3 OHA*
[3]*Jodrell Bank Centre of Astrophysics, School of Physics and Astronomy, University of Manchester, Oxford Road, Manchester M13 9PL*

Accepted 2010 August 22. Received 2010 August 20; in original form 2010 May 11

ABSTRACT

We propose a new technique for weak gravitational lensing in the radio band making use of polarization information. Since the orientation of a galaxy's polarized emission is both unaffected by lensing and is related to the galaxy's intrinsic orientation, it effectively provides information on the unlensed galaxy position angle. We derive a new weak-lensing estimator, which exploits this effect and makes full use of both the observed galaxy shapes and the estimates of the intrinsic position angles as provided by polarization. Our method has the potential both to reduce the effects of shot noise and to reduce to negligible levels, in a model-independent way, all effects of intrinsic galaxy alignments. We test our technique on simulated weak-lensing skies, including an intrinsic alignment contaminant consistent with recent observations, in three overlapping redshift bins. Adopting a standard weak-lensing analysis and ignoring intrinsic alignments results in biases of 5–10 per cent in the recovered power spectra and cosmological parameters. Applying our new estimator to one-tenth the number of galaxies used for the standard case, we recover both power spectra and the input cosmology with similar precision and with negligible residual bias. This remains true even in the presence of a substantial (astrophysical) scatter in the relationship between the observed orientation of the polarized emission and the intrinsic orientation. Assuming a reasonable polarization fraction for star-forming galaxies, and no cosmological conspiracy in the relationship between polarization direction and intrinsic morphology, our estimator should prove a valuable tool for weak-lensing analyses of forthcoming radio surveys, in particular, deep wide-field surveys with e-MERLIN, MeerKAT and ASKAP, and ultimately, definitive radio lensing surveys with the SKA.

Key words: gravitational lensing: weak – methods: analytical – methods: statistical – cosmology: theory.

1 INTRODUCTION

The bending of light by mass inhomogeneities in the Universe results in coherent distortions in the observed images of faint background galaxies. In recent times, significant progress has been achieved in measuring this weak gravitational lensing effect (see e.g. Massey, Kitching & Richard 2010 for a recent review). Weak lensing on cosmological scales (or 'cosmic shear') was first detected only 10 yr ago (Bacon, Refregier & Ellis 2000; Kaiser, Wilson & Luppino 2000; Van Waerbeke et al. 2000; Wittman et al. 2000), and has since been measured with steadily improving precision by a large number of groups (see e.g. Fu et al. 2008 for the most recent constraints from the CFHT Legacy Survey). Since the underlying physics of weak lensing is clean, future cosmic shear measurements that include distance information on the source galaxies are considered to be one of the most promising techniques for constraining the growth of cosmological fluctuations over cosmic time. Cosmic shear therefore offers great promise for constraining a variety of cosmological parameters including the amplitude of the fluctuations, neutrino masses and the properties of dark energy (e.g. Albrecht et al. 2006; Peacock et al. 2006).

In order to measure weak lensing, one must average over the observed shapes of a sufficient number of background galaxies – since one does not know, a priori, the intrinsic shape of any one galaxy, the lensing distortion cannot be recovered from a single galaxy image. If one assumes that there is no correlation in the intrinsic shapes of galaxies, then by averaging over a sufficient

⋆E-mail: mbrown@ast.cam.ac.uk (MLB); Richard.Battye@manchester.ac.uk (RAB)

number of source galaxies, one obtains an unbiased estimate of the distortion induced by lensing.

There are two caveats to this technique. First, there is both theoretical motivation (e.g. Catelan, Kamionkowski & Blandford 2001; Crittenden et al. 2001; Jing 2002; Mackey, White & Kamionkowski 2002; Hirata & Seljak 2004) and observational evidence (Brown et al. 2002; Heymans et al. 2004; Mandelbaum et al. 2006, 2009; Hirata et al. 2007; Brainerd et al. 2009) for believing that the intrinsic shapes of galaxies are not completely random. Such intrinsic shape correlations will mimic a lensing signal, introducing spurious power (the so-called intrinsic–intrinsic or 'II' term) into estimates of the autocorrelations of the lensing distortion (or 'shear') field. Moreover, intrinsic correlations can introduce spurious anticorrelations between the shear estimated from galaxies, which are widely separated in redshift (the so-called lensing-intrinsic interference or 'GI' term; Hirata & Seljak 2004). This anticorrelation arises, since the ellipticities of foreground galaxies are partly determined during the galaxy formation process by the neighbouring matter distribution, which, in turn, is also responsible for lensing background galaxies. Of these two effects, the GI term is potentially the most worrisome as it is not easily removed from cosmic shear estimators.

Secondly, even if the intrinsic shapes of galaxies are truly random, the dispersion in galaxy shapes introduces a shot noise term. Since this dispersion is very much larger than the sought-after weak-lensing signal, one requires large numbers of background galaxies in order to beat down this noise. For this reason, the vast majority of weak-lensing surveys to date have been conducted in the optical. In particular, weak lensing in the radio band has lagged behind somewhat due to the much smaller galaxy number density achieved in radio surveys. However, the next generation of radio surveys, such as the imminent e-MERLIN[1] and LOFAR (Morganti et al. 2010) experiments, the SKA pathfinders, MeerKAT (Booth et al. 2009) and ASKAP (Johnston et al. 2008), and ultimately, the SKA[2] itself, will be of sufficient sensitivity to achieve a comparable source galaxy number density to planned optical surveys.

The only significant measurement of cosmic shear in the radio band is the work of Chang, Refregier & Helfand (2004) who made a statistical detection in the VLA FIRST survey. Recently, a further attempt to measure a lensing signal was applied to data from the VLA and MERLIN (Patel et al. 2010). The latter work did not detect a significant lensing signal precisely because of the small number density of galaxies typically found in radio surveys. However, it was able to assess the feasibility of doing so and also proposed that systematic effects could be removed by observing the same patch of the sky in the radio and optical wavebands.

One aspect of radio surveys that is potentially useful for weak lensing is the additional polarization information, which often comes for free in these surveys. In particular, all of the forthcoming surveys mentioned above will include full polarization information. Numerous authors have demonstrated that, in almost all cases of astrophysical interest, the orientation of the polarized emission from a source galaxy is unaffected by gravitational lensing (Kronberg et al. 1991; Dyer & Shaver 1992; Faraoni 1993; Surpi & Harari 1999; Sereno 2005). It follows that if there exists a correlation (or anticorrelation) between the intrinsic morphological orientation of a source and its polarized emission, then the observed polarization provides information on the unlensed source orientation. Such a relationship certainly exists for quasars where the polarization is closely aligned with the radio jets and this effect has already been exploited to measure gravitational lensing using polarization observations of quasars (Kronberg et al. 1991; Kronberg, Dyer & Roeser 1996; Burns et al. 2004). The number counts of future deep radio surveys will be dominated by quiescent star-forming galaxies rather than active galactic nuclei (AGNs). Observations in the local Universe indicate that the orientation of the polarized emission from these sources is also strongly anticorrelated with the orientation of the galaxy (e.g. Stil et al. 2009).

In this paper, we construct a new weak-lensing estimator, which folds in the extra information on the intrinsic orientation of galaxies, which can potentially be provided by radio polarization observations. We demonstrate that, depending on the strength of the correlation between the polarized emission and the galaxy orientation, our proposed technique has the potential to reduce the impact of shot noise and to mitigate intrinsic alignment (IA) effects. Focusing on the potential impact for cosmic shear measurements, we test our technique on simulated weak-lensing skies, which include an IA contaminant. We demonstrate that IA biases can be reduced to negligible levels, in a model-independent way, with negligible loss in cosmological information as compared to a standard weak-lensing analysis, which uses a factor of 10 more galaxies.

Note that our proposed technique is markedly different from other techniques for mitigating the effects of IA, which are generally based on either nullifying the contaminating signals (King & Schneider 2002; Heymans & Heavens 2003; Takada & White 2004; Joachimi & Schneider 2008, 2009) or fitting parametrized models of the IA signals (e.g. King & Schneider 2003; King 2005; Bridle & King 2007). Some of the nullifying techniques are focused on removing the II term and some have been constructed to explicitly remove the GI term, while the modelling approaches attempt to model out all contaminating signals. In general, the nullifyng techniques are lossy in the sense that they discard useful cosmological information along with the IA contamination. The modelling techniques are less lossy but are dependent on our highly uncertain knowledge of the physics underlying IA effects. This model dependence can be mitigated to some degree by including empirical constraints on the IA signal, for example, by considering measurements of the cross-correlation between the galaxy number density and observed shear fields (Zhang 2010; Bernstein 2009; Joachimi & Bridle 2009; Kirk, Bridle & Schneider 2010).

All of these existing techniques remove or model the IA contamination at the two-point level (i.e. in the correlation functions or power spectra). Since the technique proposed here works directly on the shear field, it separates the IA and lensing signals at the map level. It therefore does not discriminate between II and GI contamination and can, in principle, be used to make maps (albeit noisy ones) of the IA signal as well as to directly correct the lensing shear field(s) for the effects of IA. In addition to cosmic shear, in principle, our technique can also be used to correct for IA contamination in other weak-lensing applications, for example, in lensing reconstructions of dark matter distributions around clusters and superclusters.

This paper is organized as follows. In Section 2, we review the observational evidence for a correlation between the orientation of the polarized emission and the intrinsic position angle (PA) of galaxies. In Section 3, we derive our new estimator and examine some of its properties. In Section 4, we describe our simulations of weak-lensing skies including an IA contaminant. The analysis of the simulations is presented in Section 5. We conclude by discussing

[1] http://www.merlin.ac.uk/e-merlin.
[2] http://www.skatelescope.org.

our results and their implications for future radio lensing surveys in Section 6.

2 POLARIZATION POSITION ANGLE AS A PROXY FOR THE INTRINSIC POSITION ANGLE

In this section, we will discuss the use of the polarization PA (PPA) as a proxy for the intrinsic structural PA of a radio source. At the low frequencies which we will consider (typically 1–10 GHz), the dominant source of linear polarization is expected to be synchrotron radiation due to electrons moving in magnetic fields. A measurement of the PPA gives information about the direction of the magnetic fields and, as we will discuss below, it is reasonable to suppose that this is related to the overall structure of the galaxy. The PPA measurement can be confused by Faraday rotation which would need to be extracted in any observations by *Rotation Measure Synthesis* using observations covering a wide range of frequencies (e.g. as described in Beck & Gaensler 2004).

The linear polarization of a source is usually described in terms of the Stokes parameters Q and U and the PPA, $0^\circ \leq \alpha \leq 180^\circ$, is conventionally defined as

$$\alpha = \frac{1}{2}\tan^{-1}\left(\frac{U}{Q}\right).$$

If the noise on the measurement of Q is σ_Q and that on U is σ_U, then if $\sigma_Q = \sigma_U = \sigma$, then one can show that the rms error on the measurement of α due to the instrument noise will be $\langle \Delta\alpha_{\rm N}^2 \rangle^{1/2} = \sigma/(2P)$, where $P = \sqrt{Q^2 + U^2}$ is the polarized intensity of the source. For a signal-to-noise ratio (S/N) of 3, this corresponds to $\approx 10^\circ$ and for an S/N of 5, it is $\approx 6^\circ$. We note that for low values of the S/N, the probability distribution function will be non-Gaussian. For higher S/Ns, one would expect any intrinsic dispersion to dominate. We will quantify this by the variance $\langle \Delta\alpha_{\rm int}^2 \rangle$, which we will assume is independent of the instrument noise and hence adds in quadrature.

The parameters important to quantify in order to assess the viability of our method relative to standard techniques are the mean error in the PA estimator, $\langle \Delta\alpha \rangle$, its total rms scatter, $\alpha_{\rm rms} = \langle \Delta\alpha^2 \rangle^{1/2} = \sqrt{(\sigma^2/4P^2) + \langle \Delta\alpha_{\rm int}^2 \rangle}$, and the distribution of fractional polarization $\Pi = P/I$ for total intensity I, quantified by the median fractional polarization $\Pi_{\rm med}$ and possibly some scatter. We will assume that $\langle \Delta\alpha \rangle = 0$, which will ensure that our estimator is unbiased in the absence of IAs; although there are many possible sources of astrophysical scatter in such measurements, it seems implausible that any of these will prefer any particular direction.

The emission from radio galaxies, which is relevant to us here, can be divided into two broad classes – star-forming galaxies and AGNs – and the nature of polarization will be very different in both. The expectation is that in each case the PPA will be perpendicular to the intrinsic axis of the galaxy, albeit for different reasons. The category of AGNs is often subdivided into radio-loud, jet-powered [Fanaroff–Riley type I (FR I)/Fanaroff–Riley type II (FR II)] and radio-quiet quasars. Both are often connected with elliptical morphologies. Star-forming galaxies are often categorized as either quiescent 'normal' galaxies, such as our own, or starbursts, which are undergoing an epoch of intensive star formation. The star-forming galaxies typically have spiral morphologies. AGNs are thought to dominate the source counts for $I > 1$ mJy and star-forming galaxies for $I < 10\,\mu$Jy with the transition expected to happen somewhere in between. We are interested in situations where the source density is high ($\sim 20\,{\rm arcmin}^{-2}$) in order for it to be possible to measure cosmic shear and hence we are interested in the sources with $I \approx 1\,\mu$Jy. Therefore, we are most interested in the properties of star-forming galaxies where the detected radio flux is dominated by emission from massive star formation. Unfortunately, very little is known about the polarization properties of such objects, since they are a very small fraction of the sources detected in presently available surveys. In what follows we will attempt to piece together a picture of what is known about this population from the information available in the literature.

Wilman et al. (2008) have constructed a simulated catalogue of radio sources as part of the Square Kilometre Array Design Studies (SKADS) programme.[3] This is a semi-empirical simulation of the extragalactic radio continuum sky over a $20 \times 20\,{\rm deg}^2$ area, which includes FR I, FR II, radio-quiet quasars, 'normal' and starburst galaxies. At levels of $I \approx 1\,\mu$Jy, the radio source population is dominated by star-forming ('normal' or starburst) galaxies. For the central square degree of the simulation, we find that there are $\approx$80 per cent star-forming galaxies ($\approx$72.5 per cent 'normal' and $\approx$7.5 per cent starburst galaxies) and $\approx$20 per cent AGNs. This is $\approx$50 per cent of each at $I \approx 50\,\mu$Jy and the proportion of star-forming galaxies increases for lower flux densities. For a detection threshold of 1 μJy, the median redshift of the star-forming galaxies is $\approx$2. The AGN types will act as a contaminating noise background when attempting to use the PPA as a proxy for the structural PA, since the radio emission is largely dominated by the jets in such sources and the alignment properties between the PPA and the structural axis will typically be different, although still aligned (Clarke, Kronberg & Simard-Normandin 1980). It should be possible to remove this contaminating population using a combination of indicators. These will include morphological information on the source, the use of other radio observations, for example, spectral index information or 21-cm line measurements, or information garnered from observations at other wavebands.

Stil et al. (2009) have performed a detailed study of star-forming galaxies in the local Universe. They extracted information from radio observations of a number of local spiral galaxies at 4.8 and 8.4 GHz, classifying them into three subsamples: standard nearby spirals, Virgo (in the Virgo Cluster) and barred spirals. They computed the PPAs and compared them to corresponding structural PAs deduced in the optical. They found a strong anticorrelation between the PPA and structural PA for the standard nearby spiral and Virgo samples, which is illustrated in Fig. 1 (bottom left-hand panel), where we present a histogram of the number of objects divided by the total number in the sample as a function of the acute angle ($\Delta\alpha$) between the optical PA and the direction perpendicular to the radio PPA at 4.8 GHz. This has an rms of $\langle \Delta\alpha^2 \rangle^{1/2} \approx 26\overset{\circ}{.}7$. The contribution due to this from random errors is expected to be negligible and therefore we consider this as an upper limit on $\langle \Delta\alpha_{\rm int}^2 \rangle^{1/2}$, provided we assume that the population at high redshifts is dominated by similar galaxies. The situation is much less clear for the barred spirals.

For our purposes we actually require the difference between the perpendicular to the PPA in the radio and the structural PA deduced from the total intensity distribution detected in the radio. Battye & Browne (2009) have investigated the differences between structural PAs measured in the optical from the SDSS (York et al. 2000) and in the radio from the FIRST (Becker, White & Helfand 1995). They found that, for star-forming galaxies identified photometrically or spectroscopically, the data were compatible with an rms

[3] Available at http://s-cubed.physics.ox.ac.uk.

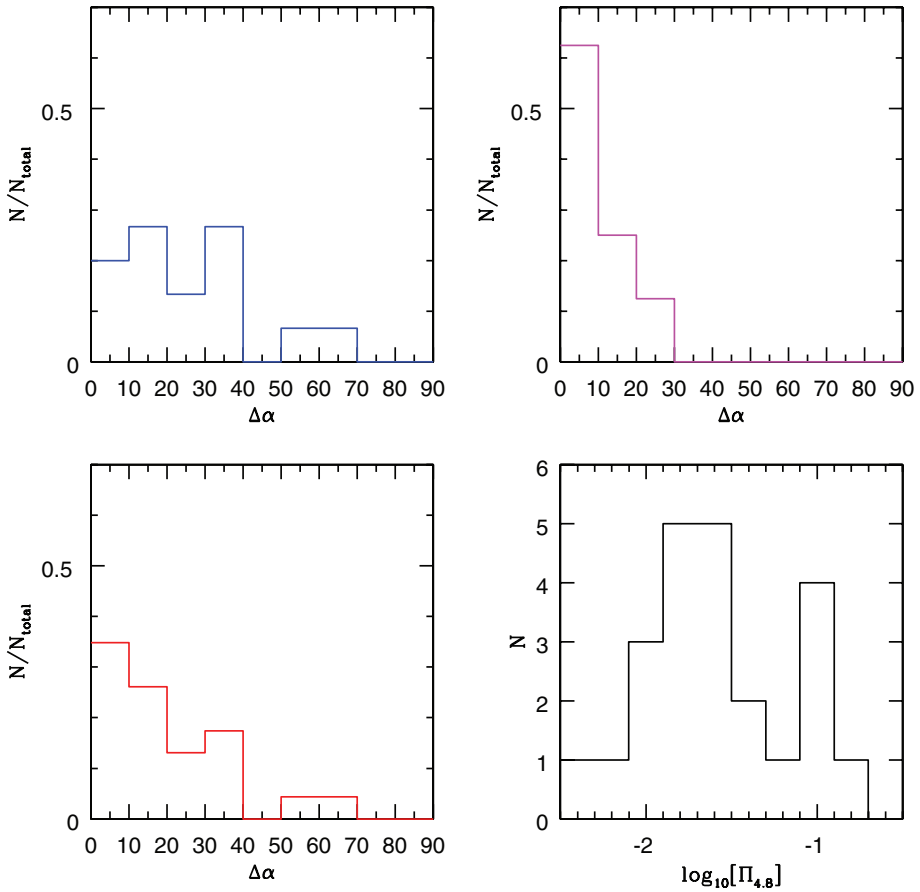

Figure 1. A summary of the results from Stil et al. (2009), presented as histograms of $\Delta\alpha$ and $\log \Pi_{4.8}$. $\Delta\alpha$ is the acute angle difference between the galaxy PA (as measured from the light distribution in the optical) and the PPA measured in the radio band. $\log \Pi_{4.8}$ is the logarithm of the polarization fraction of the galaxies at 4.8 GHz. Bottom left-hand panel: histogram of the number of objects divided by the number in the sample as a function of $\Delta\alpha$ for the nearby spiral and Virgo samples of galaxies. Bottom right-hand panel: histogram of the number of objects as a function of $\log \Pi_{4.8}$. Top left-hand panel: the equivalent of the bottom left-hand figure, but for $\Pi_{4.8} < 0.03$. Top right-hand panel: the equivalent of bottom left-hand figure, but for $\Pi_{4.8} > 0.03$.

difference which is $\approx 15^\circ$. Some of the dispersion observed by Stil et al. (2009) could be due to them using the optical PA and this could be responsible for the less-clear correlation in the barred galaxies whose estimated optical PAs could be very different from their radio PAs. Under the assumption that the PPA observed in the radio is more strongly anticorrelated with the structural PA observed in the radio than it is with the structural PA observed in the optical, and assuming that the two effects are independent, we estimate $\langle \Delta\alpha_{\rm int}^2 \rangle^{1/2} < 22.^\circ 5$.

The fractional polarization of these galaxies ($\Pi_{\rm med} = 0.024$) is typically higher than that found for AGN-type galaxies. We present a histogram of the fractional polarization of the standard nearby spiral and Virgo samples in Fig. 1 (bottom right-hand panel). There appears to be a peak around $\Pi \approx 0.1$ which might suggest a population of sources with high fractional polarization, although this is not statistically significant. We have produced histograms of $\Delta\alpha$ for $\Pi_{4.8} < 0.03$ and $\Pi_{4.8} > 0.03$, which are presented in Fig. 1 (top left-hand and top right-hand panels, respectively). For low fractional polarization, there is still a trend for $\Delta\alpha$ to be biased towards zero but with a higher dispersion $\langle \Delta\alpha^2 \rangle^{1/2} \approx 31.^\circ 7f$, whereas for higher fractional polarization, the histogram has a dispersion of only $\langle \Delta\alpha^2 \rangle^{1/2} \approx 13.^\circ 2$. The latter value would be compatible with $\langle \Delta\alpha_{\rm int}^2 \rangle \approx 0^\circ$ if the structural PA is measured from the total intensity distribution observed in the radio. Stil et al. (2009) also report an anticorrelation between fractional polarization and the luminosity measured at 4.8 GHz. They also comment that high fractional polarization is often connected with high inclination angles of the associated disc. For example, the four sources with the highest reported fractional polarization at 4.8 GHz have inclination angles in the range 75°–90°.

The anticorrelation between the structural PAs deduced in the radio and optical and the PPA is to be expected in star-forming galaxies, since radio and optical emission are both dominated by the stars in the disc of the galaxy, albeit from somewhat different star populations. The massive star formation and the magnetic field responsible for the radio emission should be aligned with the galaxy's disc and the higher is the level of alignment, the higher the fractional polarization is expected to be. This, and the observational evidence discussed in the previous paragraph, leads to the interesting conclusion that the level of intrinsic scatter in $\Delta\alpha$ will be anticorrelated with Π. This means that galaxies with higher fractional polarization, in which the polarization is easier to detect relative to lower fractional polarization counterparts, have lower values of $\langle \Delta\alpha_{\rm int}^2 \rangle$. Effectively, a subsample of galaxies selected to have high fractional polarization will have a low dispersion in the PA proxy relative to the whole sample. Note, however, that such a subsample might also suffer from an enhanced dispersion in intrinsic ellipticity, since highly inclined systems would be preferentially selected.

There is some evidence that the fractional polarization is increasing at low flux densities at 1.4 GHz (Taylor et al. 2007; Grant et al.

2010; Subrahmanyan et al. 2010). This increase appears to start around $I \approx 10$ mJy and continues at least down below $I \approx 1$ mJy. There is a general agreement that some increase takes place but disagreement about how much, although we note that the results are not incompatible, since they probe different regimes of flux density and that the discrepancies are not that significant in the regions where they overlap. Taylor et al. (2007) and Grant et al. (2010) find $\Pi_{\rm med} \approx 0.05$ for $I \approx 10$ mJy, compared to $\Pi_{\rm med} \approx 0.015$ for sources with high flux density, whereas Subrahmanyan et al. (2010) suggest $\Pi_{\rm med} \approx 0.15$ below $I \approx 1$ mJy. Since it is thought that the star-forming galaxies start to become a significant fraction of the sources around these flux densities, it is tempting to believe that this rise, however big it might be, is at least partially due to the population of star-forming galaxies, although it could equally likely be due to a hitherto unidentified population of AGNs with high fractional polarization.

An accurate measurement of the ellipticity from the total intensity will require a high-S/N detection, since it requires the measurement of three parameters – the semimajor and semiminor axes and the PA, or equivalently the quadrupole moments. Blake et al. (2007) have estimated that this will require $\approx 10\sigma$ detections. Accurate measurement of the PPA, such that the random error is comparable to the scatter expected from the work of Stil et al. (2009), probably only requires a 3–5σ detection. If, as we have attempted to argue, the median level of fractional polarization of the star-forming galaxies is $\Pi_{\rm med} \sim 0.1$, then we will get useful polarization information from $\sim$20–30 per cent of the galaxies for which an accurate measurement of the ellipticity is possible.

Clearly there is still some uncertainty in the predictions discussed above. Probably, the most important is that the population, which will be probed by observations relevant to weak lensing, will be at substantially higher redshifts than that discussed in Stil et al. (2009). At these high redshifts even 'normal galaxies' will be undergoing substantial star formation and hence the radio and optical emission, and the orientation of the polarized emission may not be as well aligned as in the local Universe. This will be investigated as part of future observational programmes leading up to the SKA.

The evidence we have discussed above presents a prima facie case that $\langle \Delta\alpha^2_{\rm int} \rangle^{1/2}$ is somewhere between 0° and about 20° and that $\Pi_{\rm med}$ could be as large as 0.1. In addition we have argued on physical grounds that $\langle \Delta\alpha^2_{\rm int} \rangle^{1/2}$ is anticorrelated with Π implying that we will preferentially select objects, which are more aligned, and that they can possibly be weighted by their fractional polarization. These assertions are, of course, uncertain and the amount of information available at present is clearly insufficient to make any strong statement. In what follows we will attempt to show how our methods depend on $\alpha_{\rm rms}$ and the number of galaxies for which we can make an accurate polarization measurement. However, for the simulations of Section 4, we are forced to pick specific values and, when necessary, we will assume that 10 per cent of the galaxies detected by the SKA will be sufficiently well detected for there to be a total rms uncertainty in the PA of $\alpha_{\rm rms} = 5^\circ$. This seems to be a reasonable balance within the range of possibilities which are discussed above.

3 SHEAR ESTIMATION WITH AN INTRINSIC PA ESTIMATE

The relationship described in the previous section between the intrinsic PA of a source galaxy and the orientation of its polarized emission effectively provides us with an estimate, however noisy, of the intrinsic PA of the galaxy. In order to fold this information into a weak-lensing analysis, a new estimator is required, which takes full advantage of the available information. In this section, we derive the appropriate estimator and present some of its properties.

3.1 Derivation

The effect of weak lensing on a background galaxy's ellipticity in the presence of photon noise is

$$\boldsymbol{\epsilon}^{\rm obs} = \boldsymbol{\epsilon}^{\rm int} + \boldsymbol{\gamma} + \boldsymbol{\epsilon}^{\rm noise}, \tag{1}$$

where $\boldsymbol{\epsilon} = \epsilon_1 + {\rm i}\epsilon_2$ is the (complex) ellipticity and $\boldsymbol{\gamma} = \gamma_1 + {\rm i}\gamma_2$ is the shear. The superscripts 'obs' and 'int' denote the observed and intrinsic ellipticity, respectively. Here we have used a definition of the ellipticity of

$$\boldsymbol{\epsilon} = \frac{Q_{11} + Q_{22} + 2{\rm i}Q_{12}}{Q_{11} + Q_{22} + 2(Q_{11}Q_{22} - Q_{12}^2)^{1/2}}, \tag{2}$$

where Q represents the (weighted) quadrupole moment of the galaxy image. Note that, depending on the definition of ellipticity used, equation (1) sometimes appears with a factor of 2 multiplying the shear (see e.g. Bartelmann & Schneider 2001 for a discussion). We can also write the ellipticity (or shear) in polar form, for example,

$$\boldsymbol{\epsilon} = |\epsilon| \exp({\rm i}\, 2\alpha), \tag{3}$$

where $|\epsilon|^2 = \epsilon_1^2 + \epsilon_2^2$ is the amplitude of the ellipticity and α is the orientation. We also have $\epsilon_1 = |\epsilon| \cos(2\alpha)$ and $\epsilon_2 = |\epsilon| \sin(2\alpha)$.

The standard estimator for the average shear field in a pixel on the sky is simply to take the average of the observed galaxy ellipticities:

$$\hat{\boldsymbol{\gamma}} = \frac{1}{N} \sum_{i=1}^{N} \boldsymbol{\epsilon}_i^{\rm obs}, \tag{4}$$

where the sum is over all galaxies falling within this pixel. From equation (1), the expectation value of this estimator is

$$\langle \hat{\boldsymbol{\gamma}} \rangle = \boldsymbol{\gamma} + \langle \boldsymbol{\epsilon}^{\rm int} \rangle + \langle \boldsymbol{\epsilon}^{\rm noise} \rangle. \tag{5}$$

For random measurement noise, $\langle \boldsymbol{\epsilon}^{\rm noise} \rangle = 0$ and in the absence of an IA signal, $\langle \boldsymbol{\epsilon}^{\rm int} \rangle = 0$. In such circumstances, equation (4) is an unbiased estimator for the average shear in a pixel. The dispersion is

$$\begin{aligned} \sigma^2_{\hat{\gamma}} &= (\langle \hat{\boldsymbol{\gamma}} \hat{\boldsymbol{\gamma}}^* \rangle - \langle \hat{\boldsymbol{\gamma}} \rangle \langle \hat{\boldsymbol{\gamma}} \rangle^*)/N \\ &= (\langle \boldsymbol{\epsilon}^{\rm int} \boldsymbol{\epsilon}^{\rm int *} \rangle + \langle \boldsymbol{\epsilon}^{\rm noise} \boldsymbol{\epsilon}^{\rm noise *} \rangle)/N, \end{aligned} \tag{6}$$

where the asterisk denotes complex conjugation. In standard weak-lensing analyses, the first term is the irreducible shot noise due to the dispersion in the (intrinsic) shapes of galaxies. Note that this is typically very much larger than the second term due to random measurement (photon) noise. In order to derive our estimator, for the remainder of this subsection, we shall assume that the measurement noise is negligible.

Writing equation (1) in component form and in terms of the intrinsic ellipticity amplitude and PA, in the absence of measurement noise, we have

$$\begin{aligned} \epsilon_1^{\rm obs} &= |\epsilon^{\rm int}| \cos(2\alpha^{\rm int}) + \gamma_1 \\ \epsilon_2^{\rm obs} &= |\epsilon^{\rm int}| \sin(2\alpha^{\rm int}) + \gamma_2. \end{aligned} \tag{7}$$

The new information coming from the orientation of the polarized emission effectively gives us a noisy estimate of the intrinsic PA, $\alpha^{\rm int}$. Even with this extra information, for a single galaxy, there are two equations and three unknowns (γ_1, γ_2 & $|\epsilon^{\rm int}|$) and so there is no unique solution. However, if we pixelize the sky and assume that the lensing shear field is approximately constant within each pixel,

then all we need is at least two galaxies in each pixel to be able to solve the system. In general, if we have N galaxies in a pixel, for each of which we have estimates of the ellipticity components ($\epsilon^{\rm obs}_{1,2}$) and intrinsic PA ($\hat{\alpha}^{\rm int}$), then we have for each galaxy

$$\epsilon^{\rm obs}_{1,i} = |\epsilon^{\rm int}_i| \cos\left(2\hat{\alpha}^{\rm int}_i\right) + \gamma_1$$
$$\epsilon^{\rm obs}_{2,i} = |\epsilon^{\rm int}_i| \sin\left(2\hat{\alpha}^{\rm int}_i\right) + \gamma_2. \quad (8)$$

Now, we have $2N$ equations and $N+2$ unknowns (γ_1, γ_2 and $|\epsilon^{\rm int}_i|$ for $i = 1, ..., N$). The system is therefore well defined and soluble – in principle, exactly. Taking the ratio of the two equations in (8) and rearranging, we have

$$\epsilon^{\rm obs}_{1,i} \sin\left(2\hat{\alpha}^{\rm int}_i\right) - \epsilon^{\rm obs}_{2,i} \cos\left(2\hat{\alpha}^{\rm int}_i\right) = \gamma_1 \sin(2\hat{\alpha}^{\rm int}_i) - \gamma_2 \cos\left(2\hat{\alpha}^{\rm int}_i\right) \quad (9)$$

Defining the pseudo-vectors,

$$\hat{\boldsymbol{n}}_i = \begin{pmatrix} \sin 2\hat{\alpha}^{\rm int}_i \\ -\cos 2\hat{\alpha}^{\rm int}_i \end{pmatrix}; \quad \boldsymbol{\epsilon}^{\rm obs}_i = \begin{pmatrix} \epsilon^{\rm obs}_{1,i} \\ \epsilon^{\rm obs}_{2,i} \end{pmatrix}; \quad \boldsymbol{\gamma} = \begin{pmatrix} \gamma_1 \\ \gamma_2 \end{pmatrix}, \quad (10)$$

equation (9) can be written in the more compact form as

$$\hat{\boldsymbol{n}}_i \cdot \boldsymbol{\epsilon}^{\rm obs}_i = \hat{\boldsymbol{n}}_i \cdot \boldsymbol{\gamma}. \quad (11)$$

Note that the vector, $\hat{\boldsymbol{n}}_i$, is simply the direction, which is at 45° to our estimate of the intrinsic PA for each galaxy.

We wish to select our estimate of the shear such that the constraint of equation (11) is enforced for each galaxy in our pixel. To achieve this, we define a χ^2 for the shear in each pixel as

$$\chi^2 = \sum_i w_i \left[\hat{\boldsymbol{n}}_i \cdot \left(\boldsymbol{\epsilon}^{\rm obs}_i - \boldsymbol{\gamma}\right)\right]^2, \quad (12)$$

where the sum is over all galaxies in a pixel and w_i is an arbitrary weight assigned to each galaxy (which should be normalized to unity). Minimizing equation (12) with respect to $\boldsymbol{\gamma}$ gives us our new estimator for the average shear in a pixel which we can write as

$$\hat{\boldsymbol{\gamma}} = \mathbf{A}^{-1}\boldsymbol{b}, \quad (13)$$

where the matrix, $\mathbf{A}$, and the vector, $\boldsymbol{b}$, are given by

$$\mathbf{A} = \sum_i w_i \hat{\boldsymbol{n}}_i \hat{\boldsymbol{n}}^T_i \quad (14)$$

$$\boldsymbol{b} = \sum_i w_i \left(\boldsymbol{\epsilon}^{\rm obs}_i \cdot \hat{\boldsymbol{n}}_i\right) \hat{\boldsymbol{n}}_i. \quad (15)$$

The matrix, $\mathbf{A}$, is simply the weighted sum of the projection matrices, $\mathbf{P}_i = \hat{\boldsymbol{n}}_i \hat{\boldsymbol{n}}^T_i$. In minimizing the χ^2 of equation (12), our estimator effectively selects the unique shear, $\hat{\boldsymbol{\gamma}}$, such that the average difference between it and the observed ellipticities, $\boldsymbol{\epsilon}_i$, projected in a direction which is at 45° to our estimates of the intrinsic PAs, is minimized.

Alternatively, if for each galaxy we rotate the coordinate system such that it is aligned with our estimate of the intrinsic PA, then the components of the observed ellipticity in this rotated (local) coordinate frame are simply

$$\epsilon^{\rm local}_{1,i} = \hat{\boldsymbol{n}}^{\parallel}_i \cdot \boldsymbol{\epsilon}^{\rm obs}_i,$$
$$\epsilon^{\rm local}_{2,i} = \hat{\boldsymbol{n}}_i \cdot \boldsymbol{\epsilon}^{\rm obs}_i, \quad (16)$$

where $\hat{\boldsymbol{n}}^{\parallel}_i = (\cos 2\hat{\alpha}^{\rm int}_i, \sin 2\hat{\alpha}^{\rm int}_i)$ is the direction parallel to the estimate of the intrinsic PA. The estimator of equation (13) thus retains the $\epsilon^{\rm local}_2$ component and discards the $\epsilon^{\rm local}_1$ component of each galaxy.

Note that one has complete freedom in choosing the weights, w_i. For example, these could be chosen in order to downweight galaxies with low-S/N polarization measurements, low fractional polarization, or to give more weight to highly regular objects whose polarization properties are extremely well understood.

3.2 Properties of the estimator

If our estimates of the intrinsic PAs ($\hat{\alpha}^{\rm int}_i$) were perfect, then it is easy to show that the estimator of equation (13) is shot noise free and would also eliminate any and all IA effects. In this case, all one would require for a sample-variance limited lensing survey insensitive to IA contamination would be two galaxies with significantly different intrinsic PAs in each sky pixel.

However, as described in Section 2, there will be an irreducible astrophysical scatter in the relationship between the true intrinsic PA and that inferred from the observed orientation of the polarized emission. This scatter will reintroduce shot noise into our estimator, the level of which is determined by the size of the scatter in $\hat{\alpha}^{\rm int}_i$ and the number density of galaxies. In the presence of an IA signal, this scatter will also result in a small residual bias in the estimator.

We show in Appendix A that, in the absence of IA signals, and for small errors in the estimates of the intrinsic PAs, $\alpha_{\rm rms} \ll 1$, the standard error is well approximated by

$$\sigma_{\hat{\gamma}} \approx 4\frac{\alpha_{\rm rms}\,\epsilon_{\rm rms}}{\sqrt{N}}, \quad (17)$$

where $\epsilon_{\rm rms} = \langle \boldsymbol{\epsilon}^{\rm int} \boldsymbol{\epsilon}^{\rm int*} \rangle^{1/2}$ is the dispersion in intrinsic ellipticities. Fig. 2 shows a comparison between this approximation and the exact numerical result. Clearly, for larger scatters ($\gtrsim 10°$) in the intrinsic PA estimates, the approximation breaks down and overestimates the true error in the estimator. In the absence of IA signals, the main impact our technique would have is in reducing the shot noise in lensing reconstruction. For example, for $\alpha_{\rm rms} = 0.08$, which corresponds to a 4.6° dispersion in the intrinsic PA estimates, one would require a factor of 10 less galaxies than that in the standard case to achieve the same level of shot noise.

In the presence of IA signals, errors in the intrinsic PA estimates will mean that the contamination is not completely removed, that is, the estimator is biased. However, we find that this bias is very much smaller than for the standard estimator. A general expression for the residual bias is hard to come by, since this bias depends on the intrinsic PAs of all the galaxies in a pixel. One therefore needs to rely on numerical simulations, but we note that the residual bias will depend on the scatter in the intrinsic PA estimates, $\alpha_{\rm rms}$, and on the IA signal itself. We note further that the residual bias is independent of both the number density of galaxies and the lensing shear signal. Fig. 3 shows the bias in the recovered shear as measured from numerical simulations as a function of both $\alpha_{\rm rms}$ and the IA signal. For an intrinsic PA scatter of $\alpha_{\rm rms} = 5°$, the bias due to IA effects is reduced by over an order of magnitude compared to the bias found in the standard estimator.

Note finally that we can construct an estimator for the IA signal trivially using the standard and new estimators:

$$\hat{\boldsymbol{\gamma}}^{\rm IA} = \hat{\boldsymbol{\gamma}}^{\rm standard} - \hat{\boldsymbol{\gamma}}^{\rm new}. \quad (18)$$

In principle, such estimates could be used as a starting point to iteratively correct for the residual bias in our shear estimator, although our simulations indicate that such a correction is unlikely to be necessary, provided that the PA estimates from polarization are good to ∼5° (see also Section 5.6).

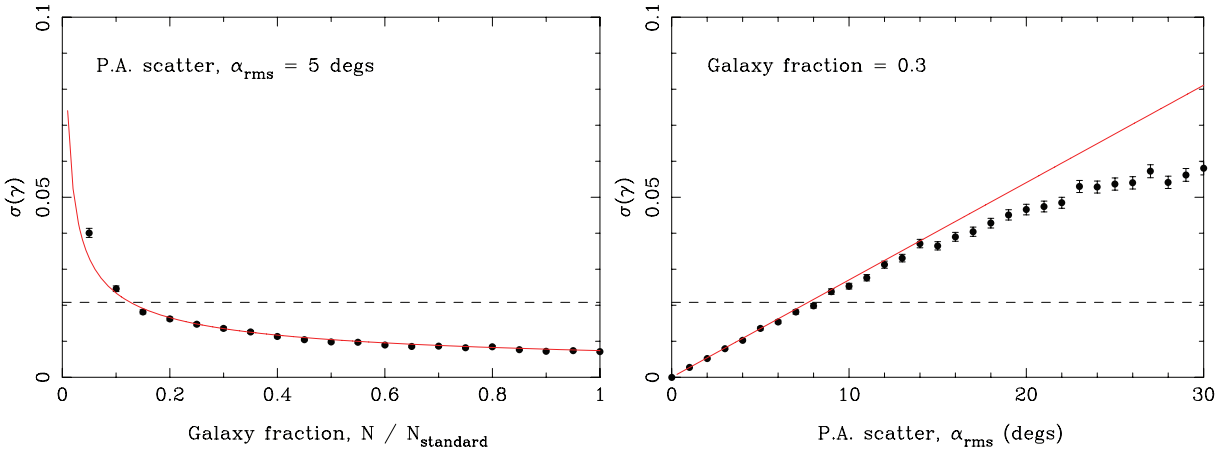

Figure 2. Left-hand panel: dispersion of the estimator (equation 13) as a function of galaxy number density for a scatter in the intrinsic PA estimates of 5°. Right-hand panel: the dispersion as a function of the scatter in the intrinsic PA estimates for a galaxy number density of 30 per cent of that used in the standard case. In both cases, the curves show the analytic approximation of equation (17), the points are the result from a numerical calculation and the dashed horizontal lines show the dispersion of the standard estimator (for $N = N_{\rm standard}$) for comparison.

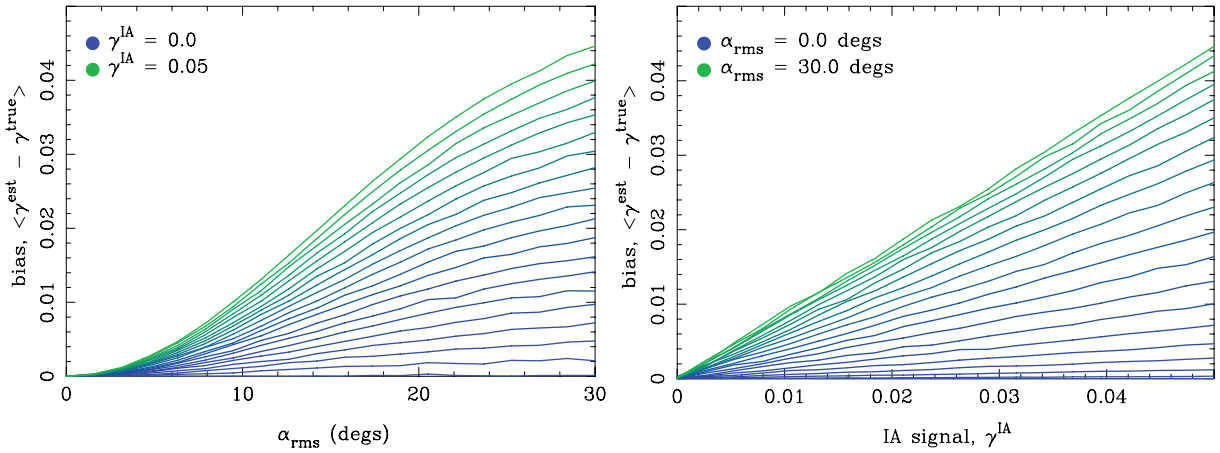

Figure 3. Residual bias in the estimator of equation (13) in the presence of an IA signal and with a non-zero error in the estimates of the intrinsic PAs. The left-hand panel shows the bias as a function of the intrinsic PA scatter for monotonically increasing IA signals. The right-hand panel shows how the bias scales with the IA signal for monotonically increasing values of $\alpha_{\rm rms}$.

4 SIMULATIONS

In this section, we will test our new estimator on simulated weak-lensing skies including a model of the IA signal. Our purpose here is to demonstrate that, given an estimate of the intrinsic PA via the polarization direction, our technique can be a potentially powerful way to minimize the impact of IA contamination in cosmic shear surveys. We have therefore not performed detailed simulations of a radio weak-lensing survey. In particular, we do not consider systematics associated with either the instrument or the atmosphere. For a comprehensive description of the possible systematics in radio surveys and their implications for weak lensing, see Chang et al. (2004). We simply note that some systematics are worse in the radio (e.g. ionospheric distortions), whereas in other cases, the reverse is true (e.g. complicated optical point spread functions versus precisely determined radio interferometer beam shapes).

We further restrict ourselves to pure Gaussian fields and ignore the non-Gaussianity of the lensing shear field on small scales. Since we consider the reconstruction of the lensing signal on medium to large scales only (multipoles, $\ell \lesssim 2000$), this should not significantly affect our conclusions.

4.1 Background cosmology and survey parameters

All of our simulations are generated within a background cosmology based on the ΛCDM cosmological model with parameters, $\Omega_{\rm m} = 0.262$, $\sigma_8 = 0.798$, $H_0 = 71.4\,{\rm km\,s^{-1}\,Mpc^{-1}}$, $\Omega_{\rm b} = 0.0443$ and $n_{\rm s} = 0.962$. We additionally assume a flat Universe, $\Omega_\Lambda = 1 - \Omega_{\rm m}$.

In what follows, we will be simulating weak-lensing and IA fields at multiple redshifts, including all possible cross-correlations between the fields at different redshifts. To limit the complexity of the system, we have therefore restricted our simulations to consider only three broad redshift bins: $0.00 < z_1 < 1.40$, $1.40 < z_2 < 2.60$ and $z_3 > 2.60$. The bin limits were chosen such that each bin contained approximately the same number density of sources. It is likely that this choice would be suboptimal for constraining cosmological parameters in the analysis of a real radio lensing data set, but we have not investigated the optimal choice in this work.

As described in Hirata & Seljak (2004), the various auto- and cross-power spectra of the weak-lensing and IA fields are given by

$$C^{\rm GG}_{\ell(ij)} = \int_0^\infty \frac{W_i(\chi) W_j(\chi)}{\chi} P_\delta(k, \chi)\, {\rm d}\chi \qquad (19)$$

$$C^{\rm II}_{\ell(ij)} = \int_0^\infty \frac{f_i(\chi) f_j(\chi)}{\chi} P_{\tilde{\gamma}^I}(k, \chi)\, {\rm d}\chi \tag{20}$$

$$C^{\rm GI}_{\ell(ij)} = \int_0^\infty \frac{W_i(\chi) f_j(\chi)}{\chi} P_{\delta,\tilde{\gamma}^I}(k, \chi)\, {\rm d}\chi, \tag{21}$$

where $k = \ell/\chi$. Here, f_i is the normalized comoving distance distribution of galaxies in bin i and $W_i(\chi)$ is the lensing selection function for the source galaxy distribution of bin i. For a lens at a comoving distance, $\chi_{\rm d}$ and with redshift, $z_{\rm d}$, the latter function can be written as

$$W_i(\chi_{\rm d}) = \frac{3}{2}\Omega_{\rm m}\frac{H_0^2}{c^2}(1+z_{\rm d})\int_{\chi_{\rm d}}^\infty f_i(\chi_{\rm s})\frac{(\chi_{\rm s}-\chi_{\rm d})}{\chi_{\rm s}}\,{\rm d}\chi_{\rm s}, \tag{22}$$

where the integration is over the distance to the source galaxies, $\chi_{\rm s}$.

In equation (19), $P_\delta(k, \chi)$ is the normal 3D matter power spectrum. To calculate this, we use the transfer function fitting formulae of Eisenstein & Hu (1999) and we use the HALOFIT code (Smith et al. 2003) to calculate the non-linear power spectrum. The two other power spectra, $P_{\tilde{\gamma}^I}(k, \chi)$ and $P_{\delta,\tilde{\gamma}^I}(k, \chi)$, are the (projected) IA power spectrum and the cross-power spectrum of the matter and IA fields, respectively. These functions are not well understood, either theoretically or observationally, which motivates a model-independent technique for removing the IA contamination. The analysis we present is a model-independent technique, but we will still need to choose an IA model to generate our simulated data sets. This is addressed in the following section.

To approximate a reasonable redshift distribution [and hence an estimate of $f_i(\chi_{\rm s})$] for future radio surveys, we make use of the SKADS simulation of Wilman et al. (2008). We select only the star-forming galaxies from this simulation down to a 1.4 GHz flux threshold of 0.5 μJy, which is a reasonable approximation to the detection threshold that might be achieved with the SKA. The normalized redshift distribution of this subset of star-forming galaxies is shown in Fig. 4. The median redshift of our $S_{1.4\,\rm GHz} > 0.5$ μJy sample is $z_{\rm m} = 2.0$ and there is also clearly a long tail to higher redshifts. If the SKADS simulation is representative of the true radio sky, then the redshifts of sources in an SKA-like lensing survey will be significantly larger than those found in planned optical lensing surveys, such as the Dark Energy Survey and EUCLID, for which the median source redshifts will be ∼1. This would obviously be good news for radio lensing as the signal would be larger on average and therefore easier to measure.

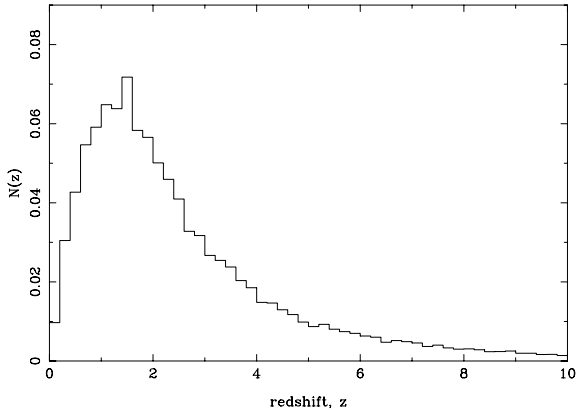

Figure 4. Normalized redshift distribution of star-forming galaxies in the SKADS simulations of Wilman et al. (2008) down to a flux threshold of $S_{1.4\,\rm GHz} = 0.5$ μJy. We consider this as the redshift distribution of the source galaxies in our simulations.

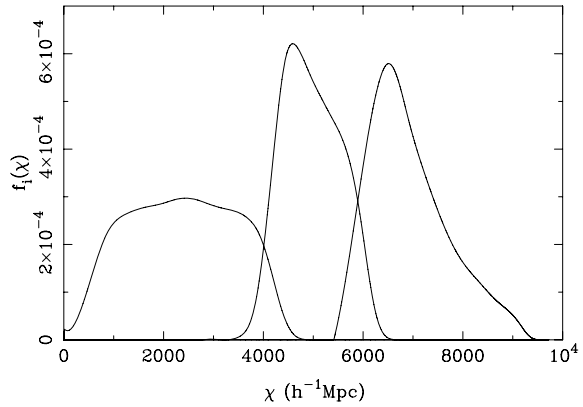

Figure 5. Normalized comoving distance distributions for our three adopted redshift bins. The overlap in the distributions is due to the redshift errors we have introduced. These overlaps in the $f(\chi)$ distributions result in non-zero expectation values for some interbin cross-correlations, which would otherwise be expected to be zero.

For the flux threshold we have applied, the total galaxy number density is ∼18 arcmin^{-2}. Following Blake et al. (2007), we note that in an SKA-like survey, precise redshift information will be available for a significant proportion of source galaxies via the detection of their H I emission. For other galaxies for which no detection of H I is obtained, photometric redshifts could potentially be provided by overlapping multiband surveys (e.g. from EUCLID). Since our present work is not focused on the effects of redshift errors, rather than attempting to mimic such a combination of redshift information, for the purpose of our simulations, we simply assign random errors to the redshifts of all sources according to $\sigma_z = (1+z)\delta_z$ with $\delta_z = 0.05$. The ultimate effect of these redshift errors will be to introduce a cross-contamination of our chosen redshift bins with objects from the neighbouring bins. The level of the contamination in our simulations is likely to be pessimistic for an SKA survey, since we have not considered the precise redshift information coming from the H I detections. Taking the redshift distribution of the star-forming galaxies from the SKADS simulation and folding in the redshift errors, the normalized selection functions for our three chosen redshift bins are shown in Fig. 5.

4.2 Model for the IA

To complete the input for our simulations, we require a model for the IA signal itself. Many authors have attempted to constrain the IA signal through theory (Catelan et al. 2001; Crittenden et al. 2001; Jing 2002; Mackey et al. 2002; Hirata & Seljak 2004), through observations (Brown et al. 2002; Heymans et al. 2004; Mandelbaum et al. 2006, 2009; Hirata et al. 2007; Brainerd et al. 2009) and by measuring the signal from numerical simulations (Croft & Metzler 2000; Heavens, Refregier & Heymans 2000; Heymans et al. 2006). Notwithstanding these efforts, our understanding of the effect is currently rather poor, mostly because the underlying physics of galaxy formation is complicated by gas dynamics, galaxy biasing and the non-linear evolution of the matter field on small scales.

One reasonably well-motivated theory is the linear alignment model of Catelan et al. (2001), which has subsequently been used to model the IA signal by a number of authors (Hirata & Seljak 2004; Bridle & King 2007). This model does not attempt to account for the non-linear evolution of the density field and so Bridle &

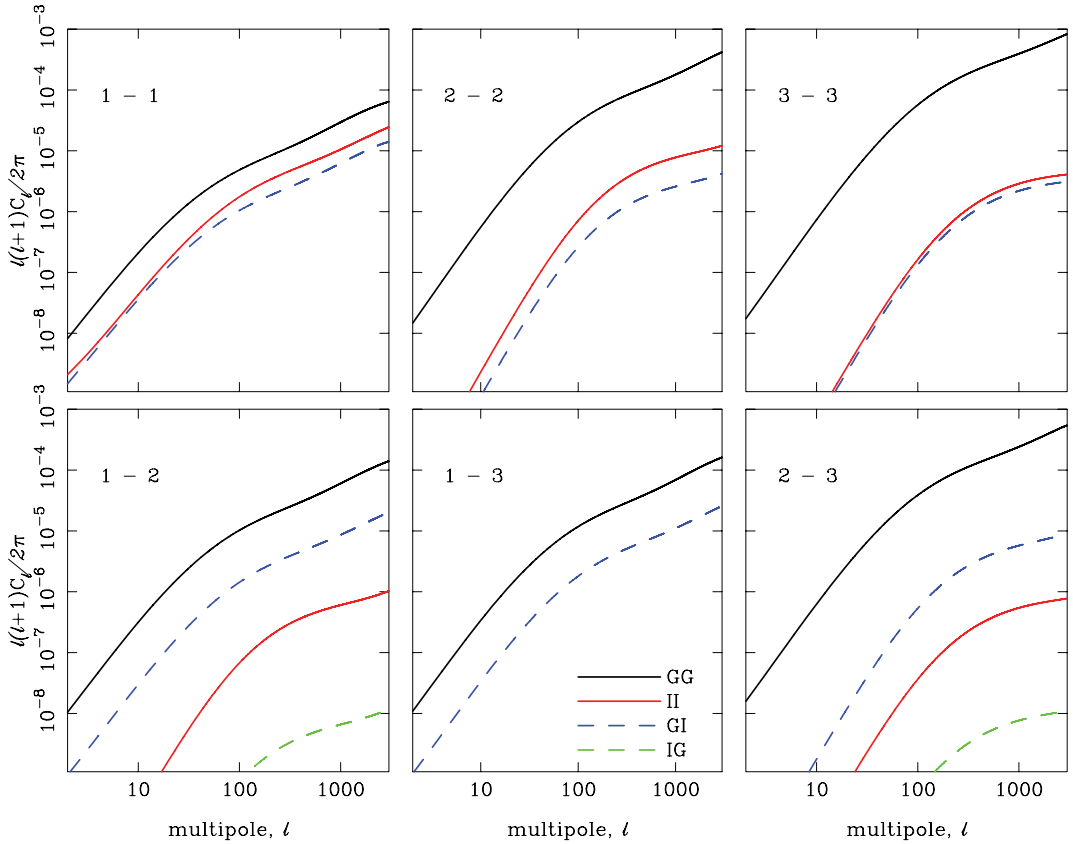

Figure 6. Input power spectra used for the simulations for the case where we have normalized the IA signal to five times the amplitude observed in the SuperCOSMOS. The title on each panel indicates which two bins are being correlated. For example, '1 - 2' means correlating fields in bin 1 with fields in bin 2. The black lines show the lensing signal. The red lines show II signals. The broken blue (and green) lines show the GI interference terms between lensing and IA. Unbroken curves are positive signals, whereas the signals shown as broken curves are negative. Note the difference between a foreground intrinsic–background shear correlation (shown as the blue lines) and a background intrinsic–foreground shear correlation (shown as the green lines). In the absence of redshift errors, the latter types of correlations, and correlations between the intrinsic fields in different redshift bins, would be expected to vanish. For example, there are no II or IG signals in the '1 - 3' panel, since the redshift distributions for these bins do not overlap (c.f. Fig. 5).

King (2007) introduced the 'non-linear linear alignment model', whereby they replaced the linear matter power spectrum with its non-linear counterpart in the linear alignment model's equations. Although it has effectively no physical motivation, this non-linear alignment model is probably as good as any other model for the IA signal available at present. Indeed, Schneider & Bridle (2010) found that a model for the IA signal based on the halo model predicts a qualitatively similar form for the IA signal. We will adopt the non-linear alignment model for our simulations, but we note again that, since our technique is model-independent, it would work just as well in the presence of any other form of IA contamination.

We use a slightly modified version of the non-linear alignment model, simplified as in Bridle & King (2007). In this model, the IA power spectrum is simply related to the matter power spectrum via

$$P_{\tilde{\gamma}^I}(k) = \frac{C_1^2\bar{\rho}^2}{\bar{D}^2} P_\delta(k), \tag{23}$$

where $\bar{D}(z) \equiv (1+z)D(z)$ is the growth factor normalized to unity at the present day and $\bar{\rho}$ is the mean matter density of the universe. The constant C_1 is a normalization constant, which Hirata & Seljak (2004) and subsequent authors have matched to the amplitude of the II signal measured in the SuperCOSMOS (Brown et al. 2002), yielding $C_1 = 5 \times 10^{-14}(h^2\,\mathrm{M}_\odot/\mathrm{Mpc}^{-3})^{-2}$. This amplitude is also consistent with constraints on the II and GI signals obtained from the SDSS (Mandelbaum et al. 2006). The cross-power between the matter and IA fields is given by

$$P_{\delta,\tilde{\gamma}^I}(k) = -\frac{C_1\bar{\rho}}{\bar{D}} P_\delta(k). \tag{24}$$

Within this model, we have $P_{\delta,\tilde{\gamma}^I}(k) = -\sqrt{P_{\tilde{\gamma}^I}(k)P_\delta(k)}$, that is, the matter and IA fields are 100 per cent anticorrelated. We will see in the next section that this property presents significant difficulties when it comes to realizing correlated 2D fields with the correct statistical properties. However, even before we consider these practical issues, heuristically, one can imagine that a perfect anticorrelation between the IA and matter fields is highly unlikely in reality due to the complicated nature of the galaxy formation process, and hence of the generation of the intrinsic correlations. We therefore slightly modify the non-linear alignment model to include a correlation coefficient, ρ_c, in the cross-power spectrum expression:

$$P_{\delta,\tilde{\gamma}^I}(k) = \rho_c \frac{C_1\bar{\rho}}{\bar{D}} P_\delta(k). \tag{25}$$

To retain the connection between the simple physical picture of the linear alignment model (Catelan et al. 2001; Hirata & Seljak 2004), we enforce the condition, $\rho_c < 0$ so that the matter and IA fields are (partially) anticorrelated and thus resulting in a negative contribution to the lensing power spectra (cf. equation 21).

We have conducted our analysis for two choices of the model parameters, C_1 and ρ_c. For our main analysis, we have used the SuperCOSMOS normalization and a correlation coefficient of $\rho_c = -0.2$. In order to demonstrate our technique on a very significant level of IA contamination, we have also considered a normalization of five times the SuperCOSMOS value, again with a correlation coefficient of $\rho_c = -0.2$. Our reason for keeping the correlation at the apparently low value of 20 per cent will be made clear in the next section. Fig. 6 shows the lensing power spectra, the IA power spectra and the cross-power spectra, calculated using equations (19)–(21), for the case where the IA normalization is five times the SuperCOSMOS value.

4.3 Simulating correlated weak-lensing and IA fields

From a set of power spectra, such as those shown in Fig. 6, we wish to generate six correlated fields, one lensing shear field and one intrinsic shear field in each of our three redshift bins. We will refer to these fields as G1, G2 and G3 for the lensing shear fields in redshift bins 1, 2 and 3 and I1, I2 and I3 for the intrinsic fields in bins 1, 2 and 3, respectively. We will work on the spherical sky and therefore use the (spin) spherical harmonic basis.

To create Gaussian realizations of all six fields with the correct correlations, at each multipole, ℓ, we construct the symmetric 6×6 power spectrum matrix, C_ℓ^{xy} where $\{x, y\} = \{\mathrm{G1}, \mathrm{G2}, \mathrm{G3}, \mathrm{I1}, \mathrm{I2}, \mathrm{I3}\}$ and the entries of the matrix are the power spectra shown in Fig. 6. Taking the Cholesky decomposition of this matrix at each multipole, L_ℓ^{xy}, defined by

$$C_\ell^{xy} = \sum_z L_\ell^{xz} L_\ell^{yz}, \tag{26}$$

we can generate random realizations of the spin-2 spherical harmonic coefficients of each field as

$$a_{\ell 0}^x = \sum_y L_\ell^{xy} G_{\ell 0}^y,$$

$$a_{\ell m}^x = \sqrt{\frac{1}{2}} \sum_y L_\ell^{xy} G_{\ell m}^y, \tag{27}$$

where $G_{\ell m}^x$ is an array of unit-norm complex Gaussian random deviates. The resulting fields transformed to real space via a spin-2 transform will then possess the desired correlations between the fields. Note that the harmonic modes of equation (27) are the even-parity E modes – in addition to assuming that the lensing signal is pure E mode, we also adopt a pure E-mode signal for the IA field, as would be expected in the linear alignment model (Catelan et al. 2001). Consequently, in all of our simulation work, we set the odd-parity B-mode component to zero.

In order for the Cholesky decomposition of equation (26) to be well defined, the power spectrum matrix must be positive-definite. More fundamentally, since the power spectrum matrix is simply the covariance matrix of the (assumed Gaussian) fields, it is a requirement that this matrix be positive semidefinite. If it is not positive semi-definite, then it is not a valid covariance matrix.

We find that when we use the unmodified non-linear (or linear) alignment IA model (equations 23 and 24), non-positive definite power spectrum matrices result. In fact, during our analysis we have found that for some configurations of redshift bins and IA signal strength, the necessary constraint, $|C_\ell^{XY}| \leq \sqrt{C_\ell^{XX} C_\ell^{YY}}$ is not satisfied or, in other words, that the two fields X and Y are more than 100 per cent (anti) correlated. These effects can be traced back to the (arguably unrealistic) 100 per cent anticorrelation between the matter and IA fields, which these models assume, and is the reason why we have introduced a correlation coefficient, $|\rho_c| \neq 1$ to describe the strength of the correlation between the matter and IA fields. The inconsistency may also be partially due to our approximating the full 3D lensing and IA fields as correlated 2D fields in three redshift bins. A detailed investigation into the degree of correlation one might reasonably expect for the IA and matter fields is beyond the scope of this paper. For the purposes of our simulations, we simply set the matter and IA fields to be anticorrelated at the 20 per cent level which, for our configuration of redshift bins, is the largest degree of correlation, which results in a positive definite power spectrum matrix at all multipoles.

Using our model for the lensing shear and IA signals, we generate the E-mode spin-spherical harmonics of all fields using equations (26) and (27) up to a maximum multipole of $\ell_{\max} = 2048$. This value was chosen in order to avoid the strongly non-linear regime as well as for computational ease. We set the B modes of all fields to zero and use fast spin-2 spherical harmonic transform routines from the HEALPIX[4] package to transform these to real space. The resulting fields are pixelized with a resolution of $\sim$3.4 arcmin (HEALPIX resolution parameter, $N_{\mathrm{side}} = 1024$).

4.4 Generating the observable fields

To simulate observable quantities, in each pixel of each redshift bin, we generate the 'observed' ellipticity of a finite number of galaxies as

$$\boldsymbol{\epsilon}^{\mathrm{obs}} = \boldsymbol{\gamma}^G + \boldsymbol{\gamma}^I + \boldsymbol{\epsilon}^{\mathrm{rand}}, \tag{28}$$

where $\boldsymbol{\gamma}^G$ and $\boldsymbol{\gamma}^I$ are the lensing and IA fields generated using the procedure described in the previous section and are the same for all galaxies within a pixel. $\boldsymbol{\epsilon}^{\mathrm{rand}}$ is the random shape noise associated with the intrinsic dispersion in galaxy ellipticities and is different for each galaxy in a pixel. For the random shape noise, we assume a Gaussian distribution with an rms ellipticity of $\boldsymbol{\epsilon}_{\mathrm{rms}} = 0.3$. We use a galaxy number density of $6\,\mathrm{arcmin}^{-2}$ for each of our three redshift bins, which were chosen to be equally populated (see Section 4.1). The total number density of galaxies for which we can measure shape information in our simulations is therefore $18\,\mathrm{arcmin}^{-2}$.

In addition to observed ellipticities for each galaxy, for our analysis including polarization information, we simulate the orientation of the observed polarized emission for a subset of the galaxies according to

$$\alpha^{\mathrm{obs}} = \alpha^{\mathrm{int}} + \alpha^{\mathrm{rand}}, \tag{29}$$

where α^{int} is the intrinsic PA of the galaxy,

$$\alpha^{\mathrm{int}} = \frac{1}{2} \tan^{-1} \left(\frac{\epsilon_2^{\mathrm{int}} + \epsilon_2^{\mathrm{rand}}}{\epsilon_1^{\mathrm{int}} + \epsilon_1^{\mathrm{rand}}} \right). \tag{30}$$

Following the discussion in Section 2, for a given instrument sensitivity, there is clearly a trade-off in how one defines the detection threshold for polarization – as one increases the threshold, the number of sources for which we have intrinsic PA information will decrease, but the noise on those PA estimates (α_{rms}) will also decrease. This behaviour will hold until the limiting irreducible astrophysical scatter in the polarization orientation–intrinsic PA relationship is reached. In a real analysis, one could envisage retaining all the galaxies in the sample for the polarization analysis and choosing the

[4] See http://healpix.jpl.nasa.gov/index.shtml and Górski et al. (2005).

weights of equations (14) and (15) based on the S/N of the polarization measurements. For our simulations, we take a simpler route and assume that we can measure the orientation of the polarized emission for 10 per cent of the galaxies in the sample and that the resulting estimates of the intrinsic PAs are subject to a combined measurement and astrophysical scatter of $\alpha_{\rm rms} = 5^\circ$. We use this value to add Gaussian noise to our intrinsic PA estimates via $\alpha^{\rm rand}$ in equation (29) and we subsequently assign uniform weights to all galaxies in our polarization subsample.

In summary, our simulated observations consist of the noisy ellipticities of galaxies containing a shear and IA signal as constructed via equation (28) and the noisy estimates of the intrinsic PAs of 10 per cent of the galaxies as constructed via equation (29).

5 ANALYSIS

In order to test the effectiveness of the technique presented in Section 3, we will reconstruct shear maps and estimate the various power spectra from our simulated observations using both the standard lensing estimator and our new technique making use of polarization information.

5.1 Shear maps

For the standard estimator, for each of our three redshift bins, we reconstruct the shear signal in each of the 3.4 arcmin pixels using equation (4). This estimator uses the full number density of simulated galaxies, that is, 6 arcmin^{-2} in each redshift bin. Of course, the reconstructed shear fields will be contaminated by the IA signal. For the new estimator, we apply equations (13)–(15) to the 10 per cent of galaxies in each pixel for which we have simulated intrinsic PA estimates. The number density used for the new estimator is therefore 0.6 galaxies arcmin^{-2} per redshift bin. As described in the previous section, we weight each galaxy equally for this analysis.

Fig. 7 shows an example of the reconstruction of the lensing signal, over a $\sim$150 deg^2 region in our highest redshift bin, projected from the spherical sky maps on to a Cartesian grid. In this redshift bin, the IA signal is negligible compared to the lensing signal and so the reconstructed maps can be directly compared to the input signal. It is clear from this figure that, for the parameters which we have adopted, the new estimator recovers the input signal with a similar precision to that achieved with the standard estimator.

5.2 Power spectrum estimation

To estimate the power spectra from the reconstructed shear maps, we use a standard pseudo-C_ℓ approach (Hivon et al. 2002; Brown, Castro & Taylor 2005). These fast power spectrum techniques have been widely used to analyse large cosmic microwave background (CMB) temperature and polarization data sets. In principle, the extension to lensing is straightforward via the transformation $\{I, Q, U, E, B\} \rightarrow \{\mu, \gamma_1, \gamma_2, \kappa, \beta\}$, where I, Q and U are the Stokes parameters of the CMB field and μ, γ_1 and γ_2 are the magnification and shear components of the lensing fields. E and κ denote the even parity E modes of the CMB polarization and lensing fields, respectively (where for the latter, we can further identify the E modes as the lensing convergence field). B and β are the odd-parity B modes of the CMB polarization and lensing fields, respectively. For lensing, we do not expect a significant cosmological signal in β and so we ignore the B modes in the analysis, which follows.

Although we do not address them in this paper, we note that, in practice, there are a number of real-world issues, which make the extension of pseudo-C_ℓ power spectrum estimators to weak lensing more problematic. Most importantly, in contrast to the simple apodizing masks usually adopted in CMB analyses, lensing analyses typically involve complicated and highly irregular masking of the data to remove diffraction spikes from bright stars and other localized contamination. Defining the optimal mask for such complicated survey geometries is not trivial (although see Hikage et al. 2010 for a recent investigation into some of these issues). In the simulations which follow, while acknowledging that a full-sky lensing survey is unrealistic, we avoid all of these issues, including any $E \leftrightarrow B$ mixing effects by working on the full (and complete) sky.

Our estimated shear maps are first transformed to spherical harmonic space using the HEALPIX spin-2 transform routines. We discard the B modes (which are consistent with noise) and by taking

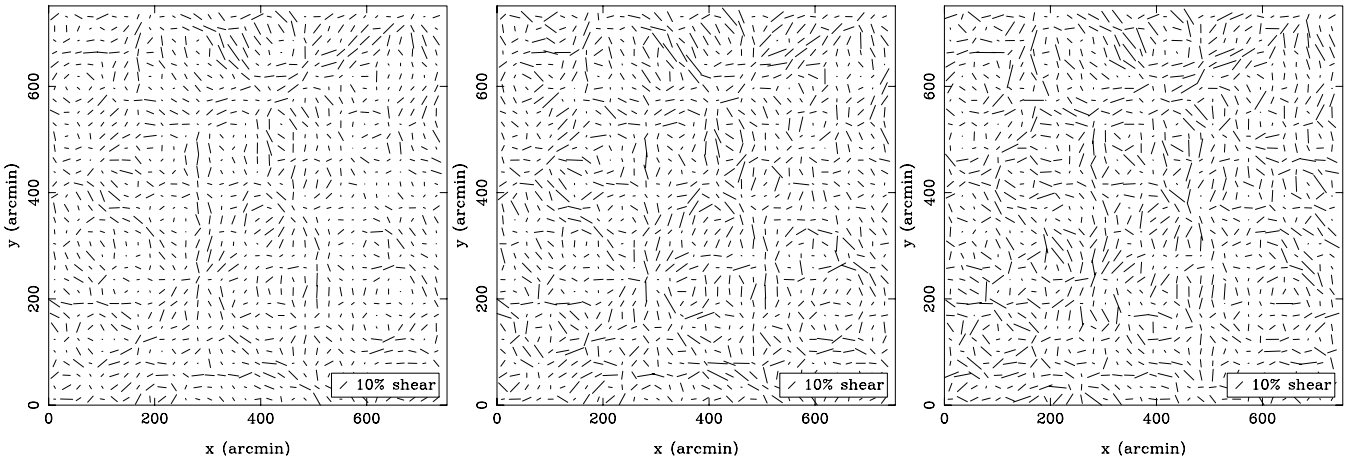

Figure 7. Example of the reconstruction of the shear signal for our highest redshift bin. The input signal is shown in the left-hand panel. The central panel shows the reconstructed signal using the standard estimator using a galaxy number density of 6 arcmin^{-2}. The right-hand panel shows the reconstruction using the new estimator with a factor of 10 less galaxies and for a scatter in the intrinsic PA estimates of 5°. For this plot, we have resampled the shear signals from the spherical sky on to a 12.5 × 12.5-deg^2 Cartesian grid with a pixel size 4.5 arcmin.

averages of the harmonic E modes of the maps, one can estimate the pseudo-C_ℓ power spectra, $\tilde{C}_\ell^{XY}$, via

$$\tilde{C}_\ell^{XY} = \frac{1}{2\ell+1}\sum_{m=-\ell}^{m=+\ell} a_{\ell m}^X a_{\ell m}^{Y\,*}, \tag{31}$$

where X and Y denote the two fields being correlated and the asterisk denotes complex conjugation. For noise-free observations over the full sky, the power spectra estimated via equation (31) should be unbiased (apart from the effect of the map pixelization which we correct for). In the presence of noise (but still on the full sky), the expectation value of this estimator is usually taken to be

$$\left\langle \tilde{C}_\ell^{XY} \right\rangle = C_\ell^{X_\mathrm{s}Y_\mathrm{s}} + C_\ell^{X_\mathrm{n}Y_\mathrm{n}}, \tag{32}$$

where $C_\ell^{X_\mathrm{s}Y_\mathrm{s}}$ is the true cosmological signal and $C_\ell^{X_\mathrm{n}Y_\mathrm{n}}$ is the power spectrum of the noise. A correction is therefore usually applied by measuring the noise bias, $C_\ell^{X_\mathrm{n}Y_\mathrm{n}}$ from a suite of noise-only simulations and subsequently subtracting this from the measured spectra:

$$\hat{C}_\ell^{XY} = \tilde{C}^{XY} - \left\langle C_\ell^{X_\mathrm{n}Y_\mathrm{n}} \right\rangle_\mathrm{mc}, \tag{33}$$

where the angled brackets denote an average over Monte Carlo simulations containing only noise. For the standard estimator, these noise-only simulations consist of just the random noise in the galaxy ellipticities. For the new estimator, they consist of both the random ellipticity noise and the random noise in the intrinsic PA estimates.

We use power spectra estimated using equation (33) as our main diagnostic for assessing the impact of IA contamination and the effectiveness of our new lensing estimator in removing it. Once estimated, we bin the values of C_ℓ into 32 equal-width flat bandpowers (denoted P_b) spanning our entire multipole range ($2 < \ell < 2048$). Since the lensing (and IA) power spectra do not exhibit any significant features over ℓ ranges comparable to our bin size ($\Delta\ell = 64$), we effectively lose no information by performing this binning, but the plots are much less cluttered and easier to interpret.

Finally, the covariance matrix of the bandpowers can be estimated from the scatter among a suite of (in our case, 200) Monte Carlo simulations:

$$\left\langle \Delta P_b^X \Delta P_{b'}^Y \right\rangle = \left\langle \left(P_b^X - \overline{P}_b^X \right) \left(P_{b'}^Y - \overline{P}_{b'}^Y \right) \right\rangle_\mathrm{mc}, \tag{34}$$

where the overline denotes the mean over all simulations.

5.3 Lensing power spectrum results

The power spectrum results for the case where the IA signal was normalized to the amplitude seen in the SuperCOSMOS are shown in Fig. 8. For this level of IA contamination, the biases in the power spectra are rather small compared to the range in amplitude of the lensing spectra over our full multipole range. In Fig. 8, instead of plotting the power spectra themselves, we therefore plot the fractional bias, $\Delta C_\ell / C_\ell^\mathrm{input}$, where ΔC_ℓ is the difference between the mean recovered spectra and the input model. Comparing the results from the standard and new estimators, we see that our technique has successfully reduced the IA bias in each spectrum by over an order of magnitude on all scales. The mean fractional bias across all multipoles for each spectrum for the standard and new estimators are presented in Table 1. There is a small residual bias in the

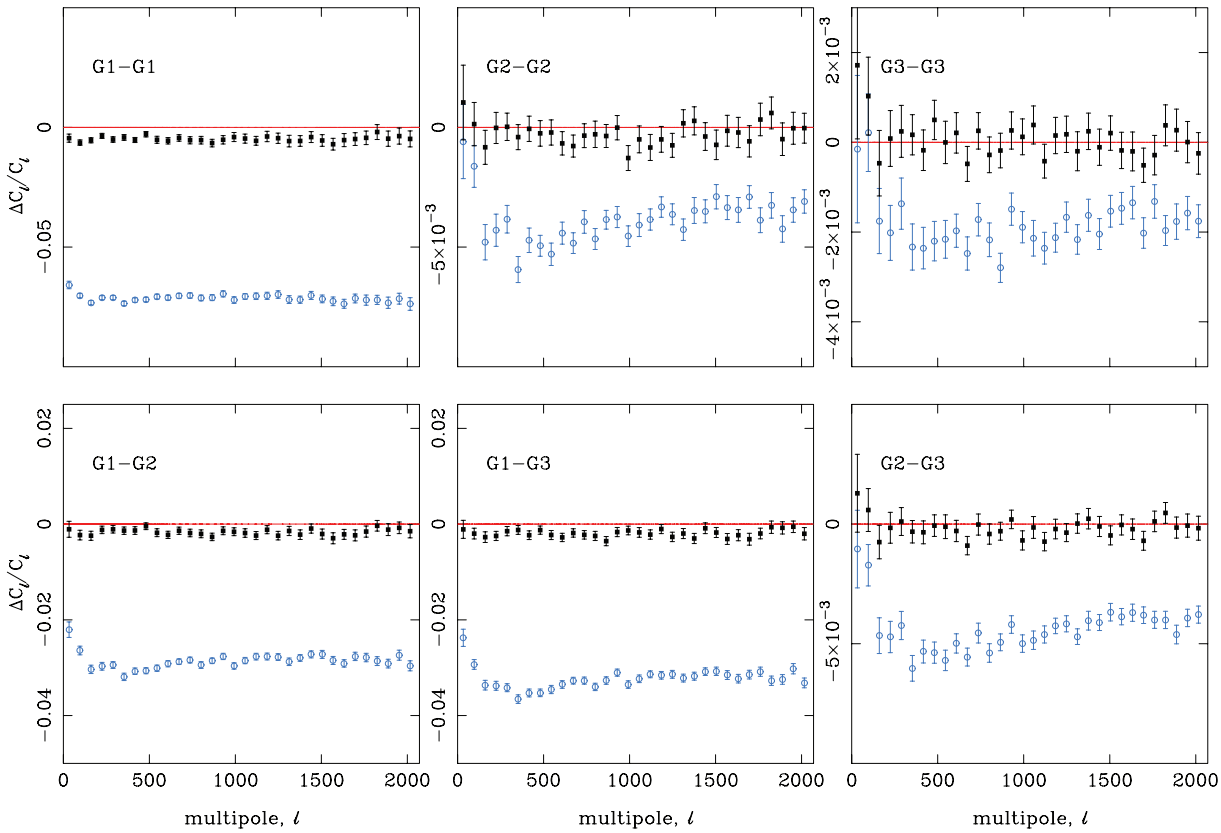

Figure 8. Fractional bias in the reconstruction of the lensing power spectra for the standard estimator (light blue points) and for the new estimator including polarization information (black points). These results are for the simulations, where the amplitude of the IA contamination was set to the level seen in the SuperCOSMOS. Once again, a factor of 10 less galaxies were used for the new estimator and we assumed an intrinsic PA scatter of 5°. For all six spectra, the average reduction in the bias is more than an order of magnitude.

Table 1. Mean fractional bias across all multipoles in the recovered lensing power spectra for the standard and new shear estimators. The first set of numbers report the biases in simulations, where the IA signal is normalized to the amplitude seen in the SuperCOSMOS. The second set of numbers are for an IA signal five times larger.

Spectrum	Standard estimator	New estimator
$1 \times$ SuperCOSMOS		
G1–G1	-7.14×10^{-2}	-4.85×10^{-3}
G2–G2	-3.84×10^{-3}	-2.55×10^{-4}
G3–G3	-1.80×10^{-3}	8.38×10^{-5}
G1–G2	-2.85×10^{-2}	-1.67×10^{-3}
G1–G3	-3.23×10^{-2}	-1.95×10^{-3}
G2–G3	-4.36×10^{-3}	-1.45×10^{-4}
$5 \times$ SuperCOSMOS		
G1–G1	-6.34×10^{-2}	-2.26×10^{-2}
G2–G2	1.27×10^{-2}	-1.30×10^{-3}
G3–G3	-3.31×10^{-3}	-5.40×10^{-4}
G1–G2	-1.34×10^{-1}	-8.43×10^{-3}
G1–G3	-1.60×10^{-1}	-9.40×10^{-3}
G2–G3	-1.97×10^{-2}	-1.33×10^{-3}

spectra recovered using the new estimator but, as we shall see in Section 5.5, this has a negligible impact on our inferences regarding the underlying cosmology. (Note that the error bars presented in Fig. 8 are the errors on the mean recovered spectra, not those for a single realization which would be $\sqrt{200}$ larger.)

In Table 1, we also present the fractional biases in the recovered power spectra for our simulations, which included an IA signal normalized to five times the signal seen in the SuperCOSMOS. For the majority of the spectra, using the new estimator, the bias is once again reduced by a factor of 10 or more. The exception is for the auto-power measured in our lowest redshift bin where the bias is reduced by only a factor of $\sim$3. The reason for this relatively poor performance is related to the apparent anomaly that the bias in the standard estimator decreases when we increase the amplitude of the IA contamination by a factor of 5. This effect is, in fact, due to a fortuitous part-cancellation of the positive II and negative GI signals within our lowest redshift bin when using the standard estimator. This cancellation is stronger in our simulations for the higher amplitude IA signal. Obviously, since such cancellations are in no way guaranteed and are highly dependent on both the details of the IA signals and the choice of redshift binning, we argue that the result for the G1 $-$ G1 bias in the standard case for the larger IA amplitude is misleadingly low. Furthermore, comparing between the numbers for the two sets of simulations, we see that for the new estimator, the residual bias increases by a factor of $\sim$5 when we increase the IA amplitude by a factor of 5, suggesting that the degree to which the IA signal is removed using the new estimator is independent of the IA model.

5.4 Intrinsic alignment reconstruction

In addition to the lensing signal, a combination of the standard and new shear estimators gives us an estimate of the IA signal itself via equation (18). In the limit of perfect intrinsic PA measurements, our new lensing estimator would be entirely shot noise free. However, this is not the case for estimates of the IA signal, which are subject to the shot noise of the standard estimator. This noise will be increased further due to the errors in the PA estimates. Since this noise is very much larger than the IA signal, our reconstructed IA maps are noise-dominated and are not particularly informative. However, we can still usefully constrain the IA signal in the power spectrum.

Fig. 9 shows the simultaneous reconstruction of the lensing spectra, the IA spectra and the lensing–IA cross-correlations for the case where we have normalized to five times the SuperCOSMOS level. All of these spectra have been estimated from the reconstructed lensing and IA maps using the normal pseudo-C_ℓ estimator of equation (33). For the lensing spectra, we also plot the recovered signal from the standard lensing estimator for comparison. Examining the IA spectra and the lensing-IA cross-correlations, we see a biased reconstruction. The source of this bias is the same as for the biases already seen in the recovered lensing signal – effectively, it is an additional 'noise bias' caused by the presence of the IA signal itself and the noise in our intrinsic PA estimates. Despite the bias, we see that the general form of the IA signals and the lensing-IA cross-correlations is recovered rather well – the residual fractional bias is fairly constant across multipoles for all spectra. Such reconstructions of the IA signal with future data sets could potentially provide much-needed observational constraints on theoretical models of the IA signal.

5.5 Parameter constraints

We consider the power spectrum results of Section 5.3 as the main diagnostic of the performance of the new estimator in removing a potential IA contaminant. It is also interesting, however, to examine the impact of our new technique on the reduction of biases in cosmological parameter constraints. As already pointed out, our simulations are clearly unrealistic in that they assume full and complete sky coverage. In addition, to conduct our analysis, we have also had to adopt values for some parameters, which are currently very uncertain. In addition to the amplitude and form of the IA signal, these include the typical fractional polarization of faint star-forming galaxies and the strength of the correlation between the orientation of the polarized emission and intrinsic morphologies of these galaxies. Consequently, the constraints on parameters obtained from these simulations will very likely be overoptimistic. We therefore emphasize that the purpose of this section is not to make parameter forecasts for lensing surveys with the SKA or any other instrument; rather, our purpose here is simply to demonstrate that our proposed technique could potentially have a large impact in terms of minimizing biases in cosmological constraints from future radio lensing surveys.

We adopt a very simple approach and perform a standard grid-based likelihood analysis in three cosmological parameters, which cosmic shear measurements can strongly constrain – the matter density ($\Omega_{\rm m}$), the power spectrum normalization (σ_8) and the (assumed constant) equation of state of the dark energy (w). We enforce a flat Universe ($\Omega_\Lambda = 1 - \Omega_{\rm m}$) and keep all other parameters fixed at their fiducial values (see Section 4.1). As our 'data', we use only the six lensing power spectra constrained in Section 5.3 and we perform the analysis for the mean power spectra estimated using both the standard and new estimators. Ordering these spectra into a $6 \times N_{\rm band}$ data vector ($\boldsymbol{d}$), we calculate the likelihood at each point in parameter space according to

$$-2 \ln \mathcal{L} = (\boldsymbol{d} - \boldsymbol{d}^{\rm th}) \mathbf{C}^{-1} (\boldsymbol{d} - \boldsymbol{d}^{\rm th})^{\rm T}, \quad (35)$$

where $\boldsymbol{d}^{\rm th}$ are the model power spectra binned in the same way as our simulated data. The covariance matrix, $\mathbf{C}$, is calculated from the simulations according to equation (34), but we retain only the diagonal elements and all same-bin interspectrum covariances. The remainder of the covariance matrix is set to zero, since these

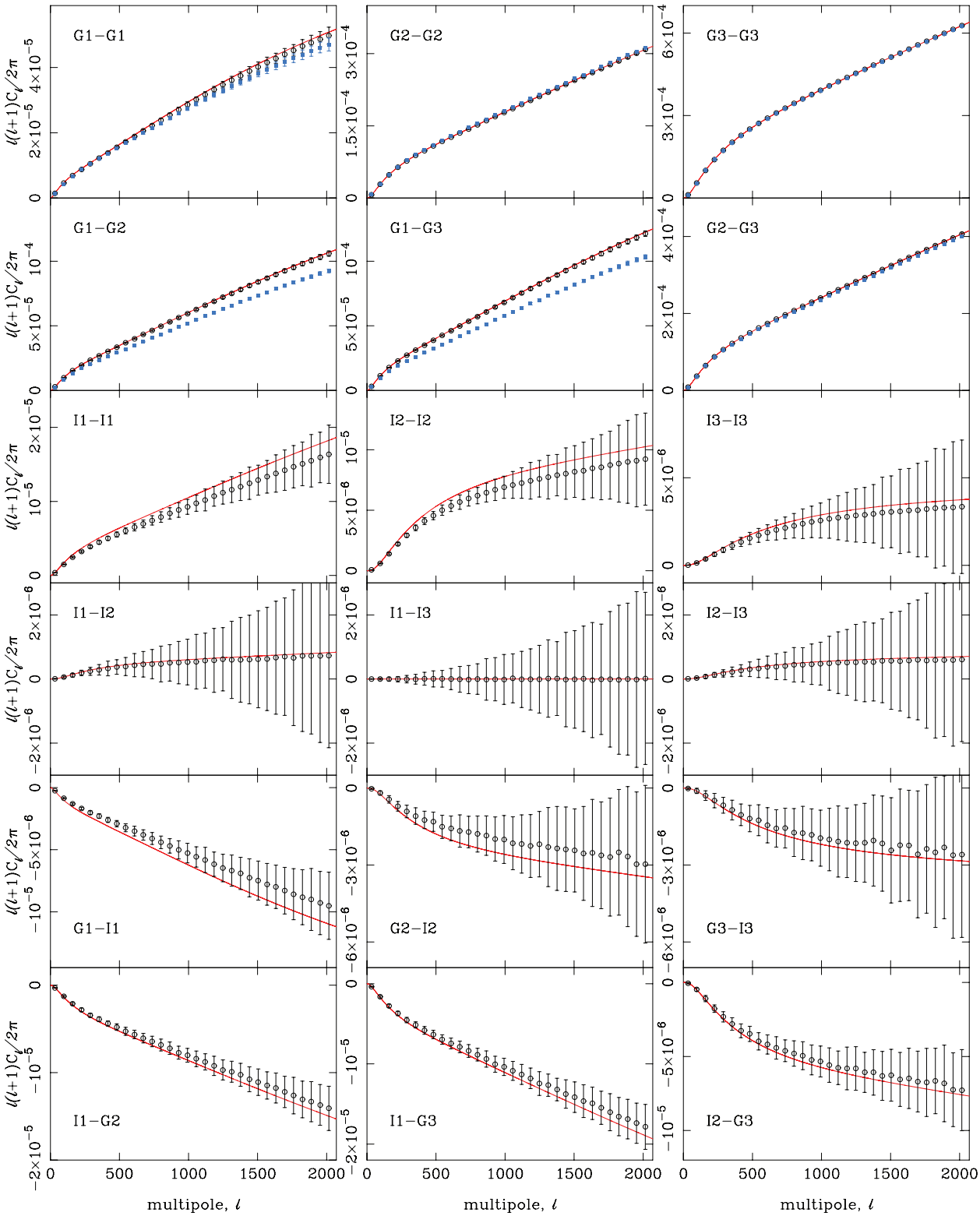

Figure 9. Reconstruction of the lensing, IA and cross-correlation signals for an IA amplitude of five times the SuperCOSMOS level. The input model spectra are shown as the smooth curves. For the lensing spectra (top two rows), the standard estimator measurements are shown as the light blue points, and the spectra measured using the new estimator are shown as the black points (for the higher redshift correlations, where the lensing signal dominates, the two sets of points are indistinguishable on this plot). The other panels show the reconstruction of the IA spectra and lensing–IA cross-correlations using a combination of the standard and new estimators. The points show the mean recovered spectra averaged over all simulations and the error bars are those appropriate for a single realization. We omit the reconstruction of the foreground shear-background intrinsic cross-correlations as these signals are very small and effectively unconstrained in our simulations (cf. the dashed green curves in Fig. 6).

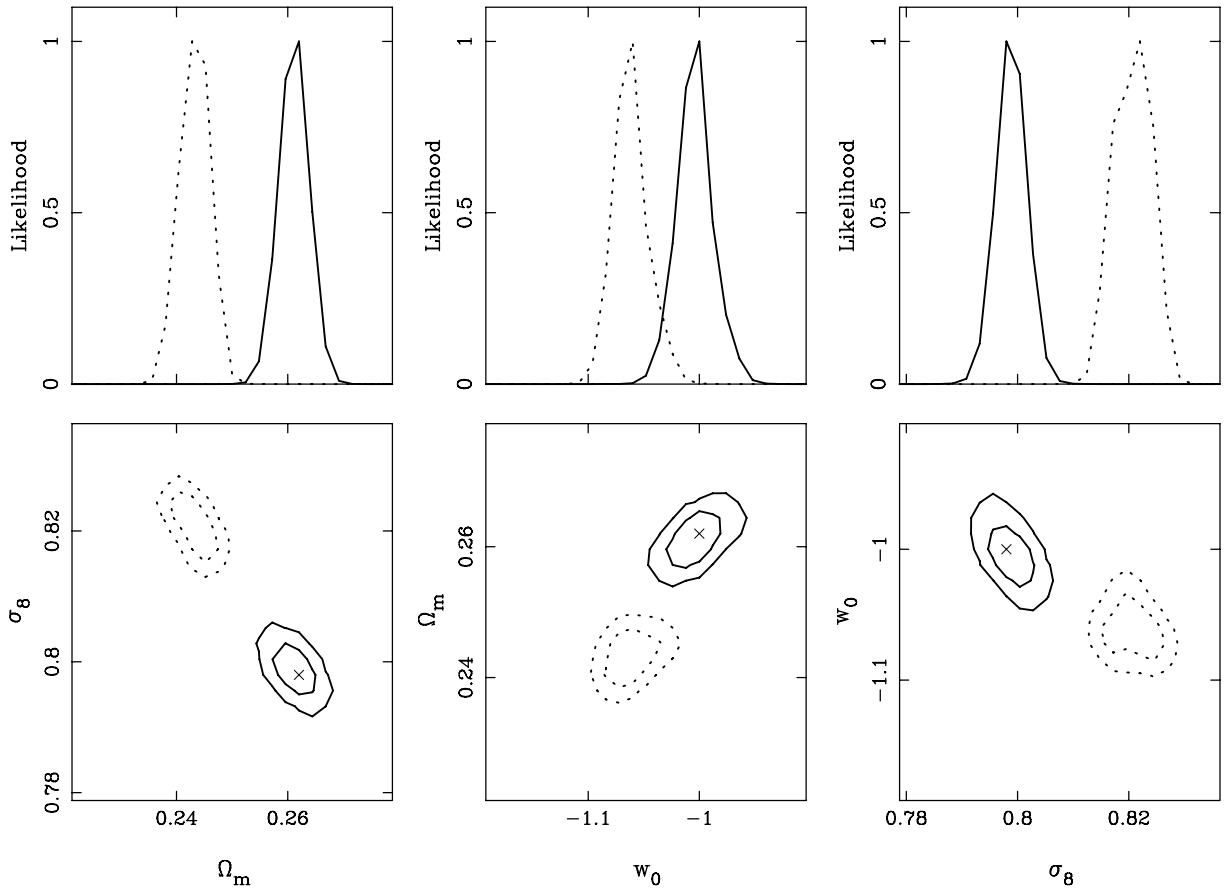

Figure 10. Marginalized 1D and 2D parameter constraints recovered from simulations, where the IA contamination is of the order of that seen in the SuperCOSMOS. For our maximum-likelihood analysis, we have only varied the three parameters, Ω_m, w and σ_8. Constraints marginalized over other parameters would be weaker. The dotted lines show the constraints obtained using the standard estimator. The full lines show the constraints using our new estimator and a factor of 10 less galaxies. The input model is indicated in the lower panels with a cross. Including the polarization reduces parameter biases to negligible levels with essentially no increase in errors. For the 2D constraints, the contours indicate the 68 and 95 per cent confidence regions.

elements are non-zero only because of numerical noise from the finite number of simulations. (Since our simulations are on the full sky, measurements at different multipoles will be uncorrelated.)

The resulting 1D and 2D parameter constraints are shown in Fig. 10 for the simulations where the IA signal was set to the level seen in the SuperCOSMOS. For the 1D constraints, we have marginalized over the other two parameters, which are varied, and for the 2D constraints, we have marginalized over the single remaining parameter. In addition to the caveats, we mention above regarding the unrealistic aspects of our simulations, we note that constraints marginalized over additional parameters, or those obtained in an extended parameter space, would obviously be weaker. We see that for all three parameters, using the standard estimator results in very significant biases in the constraints obtained. Moreover, the size of the biases seen in Fig. 10 are at least as large as the 1σ uncertainties in cosmological parameters expected to be achieved with the 'Stage IV' dark energy projects identified by the Dark Energy Task Force (Albrecht et al. 2006) including the SKA.

The biases are reduced to negligible levels when we use the power spectra obtained with the new shear estimator. For the latter case, the maximum-likelihood model corresponds to the input model. Note that the size of the errors are not particularly informative (due to the caveats we have already mentioned), but the relative size of the errors for the standard and new shear estimator cases is relevant and is extremely encouraging, that is, the bias due to the IA contamination has been removed (essentially completely) with effectively no loss in cosmological information.

We have also performed the likelihood analysis for the simulations with the much larger IA normalization. In this case, there are residual $\sim 1\sigma$ biases in the parameters obtained with the new estimator, but the degree to which the contamination is reduced from the standard estimator case is similar to that seen in Fig. 10.

5.6 A procedure to correct for residual bias

Although the results of the previous sections are encouraging, ideally one would prefer a completely unbiased and model-independent technique for removing IA signals from lensing surveys. Here we suggest an iterative technique, which is only mildly model-dependent, to correct for the residual biases seen in the previous sections.

The expectation values for the pseudo-C_ℓ power spectra as written in equation (32) assume that there is no correlation between the signal and the noise and this is usually the case. However, as described in Section 3, in the presence of a non-zero IA signal and a non-zero error on our estimates of the intrinsic PAs, there will be an extra 'noise bias' in our estimates of the shear in each pixel. This bias depends on the IA signal (see Fig. 3). Although our noise-only simulations include the noise on the intrinsic PA estimates, they do not account for this extra bias, since the IA signal is not present

in these simulations. The residual biases in the power spectra can effectively be eliminated by including an estimate of the IA signal in the noise-only simulations. In addition, since non-zero IA signals partly determine the noise in the shear estimator, we also need to consider correlations between the signal and the noise in addition to the usual autocorrelations of the noise.

In the most general case, we can write the expectation value of equation (31) as

$$\left\langle \tilde{C}_\ell^{XY} \right\rangle = C_\ell^{X_\mathrm{s}Y_\mathrm{s}} + C_\ell^{X_\mathrm{n}Y_\mathrm{n}} + C_\ell^{X_\mathrm{s}Y_\mathrm{n}} + C_\ell^{X_\mathrm{n}Y_\mathrm{s}}, \tag{36}$$

and one can construct estimators for the various power spectra, which will always be formally unbiased as

$$\hat{C}_\ell^{XY} = \tilde{C}_\ell^{XY} - \left\langle C_\ell^{X_\mathrm{n}Y_\mathrm{n}} \right\rangle_\mathrm{mc} - \left\langle C_\ell^{X_\mathrm{s}Y_\mathrm{n}} \right\rangle_\mathrm{mc} - \left\langle C_\ell^{X_\mathrm{n}Y_\mathrm{s}} \right\rangle_\mathrm{mc}. \tag{37}$$

Of course, in order to estimate quantities, such as $\langle C_\ell^{X_\mathrm{s}Y_\mathrm{n}} \rangle_\mathrm{mc}$, from simulations, one requires a model for the signal component of these simulations. We have confirmed that using equation (37) returns completely unbiased results for all of the power spectra shown in Fig. 9, provided we use the correct model for the IA signal in the noise-only simulations. The power spectrum estimators of Section 5.2 already provide us with an initial estimate of the IA signal. An iterative technique thus presents itself whereby one could fit a theoretical model (or alternatively use a 'model-independent' spline fit) to the initial power spectrum estimates of the previous sections and then use the best-fitting model as an input IA signal into the noise-only simulations. Updated estimates of the power spectra could then be obtained using equation (37) and the process iterated until subsequent iterations of the estimated power spectra were deemed consistent. Although we have not tested this proposed technique, since the recovered IA signal is already very close to the true model in Fig. 9, it seems likely that a single iteration would be sufficient to reduce the residual bias to a level well below the statistical noise.

6 DISCUSSION

Future deep, wide-field radio surveys will present a significant opportunity to measure weak lensing in the radio band with high precision for the first time. For such precise measurements, the effects of IAs can no longer be ignored. In this paper, we have presented a technique to mitigate against IA contaminants in radio weak-lensing analyses, which makes use of the fact that the orientation of the polarized emission from background sources is both unaffected by gravitational lensing and related to the intrinsic morphological orientation of the source.

We have demonstrated the technique on simulated weak lensing skies including a contaminating IA signal. The results of these tests suggest that our method has the potential to both reduce shot noise and to strongly reject IA contamination, in a model-independent way, with negligible loss in cosmological information. We note that there are a number of limitations to the simulations presented in this paper. In particular, we have approximated the lensing shear signal as being constant for all galaxies within each pixel of each of our three redshift bins. Of course, in reality, the shear undergone by each galaxy will depend on both its angular position within the pixel and its redshift. This is, however, not an obstacle for our proposed technique. In the absence of IA signals, it is easy to show that our new estimator for the shear in each pixel simply returns a weighted average of the shears sampled at each galaxy position when those shears are different. This average shear is, of course, the cosmological observable of interest – the effects of subpixel gradients in the true shear field and the dependence on redshift of the average shear field are easily accounted for when generating model predictions for comparison with observations. In the presence of both a scatter in the intrinsic PA estimates and a non-zero IA signal, there remains a residual bias in the estimator. However, we have already demonstrated that this bias is small and, if necessary, could be corrected for.

Although we have presented our technique in the context of weak lensing in the radio band, an extension to other wavebands, and in particular to the optical, is in principle possible and would be highly desirable. In this regard, Audit & Simmons (1999) have already suggested that the orientation of the optical polarized emission from a galaxy also provides a proxy for the galaxy's intrinsic orientation. However, the underlying mechanism for the generation of the polarization is quite different between the radio and optical bands – in the former case, the dominant source of polarization is synchrotron radiation, whereas in the latter case, scattering by dust can also be an appreciable source. In addition, sensitive polarization measurements are more difficult, from an instrumental point of view, in the optical band.

Our proposed technique is clearly dependent on the true nature of the polarized emission from the faint star-forming galaxies which will dominate the number counts of future radio surveys. In particular, the typical polarization fraction of such galaxies at μJy flux densities and the degree to which the orientation of the polarized emission is aligned with the morphological orientation are currently very uncertain. In addition, to apply our analysis to real data, we will need to correct the observed polarization for the rotation of the plane of polarization due to intervening cosmological magnetic fields and the effects of Faraday rotation internal to the sources themselves. These corrections should be possible by extracting the rotation measures for the sources using multifrequency information. We hope to investigate many of these practical issues and perform the first application of our proposed technique on powerful new radio data sets from the imminent e-MERLIN and MeerKAT instruments in the not-too-distant future.

ACKNOWLEDGMENTS

We are grateful to Paddy Leahy, Ian Browne, Neal Jackson, Anthony Challinor and Lindsay King for useful discussions. The simulation work described in this paper was carried out on the University of Cambridge's distributed computing facility, CAMGRID. We acknowledge the use of the HEALPIX (Górski et al. 2005) package.

REFERENCES

Albrecht A. et al., 2006, preprint (astro-ph/0609591)
Audit E., Simmons J. F. L., 1999, MNRAS, 303, 87
Bacon D. J., Refregier A. R., Ellis R. S., 2000, MNRAS, 318, 625
Bartelmann M., Schneider P., 2001, Phys. Rep., 340, 291
Battye R. A., Browne I. W. B., 2009, MNRAS, 399, 1888
Beck R., Gaensler B. M., 2004, New Astron. Rev., 48, 1289
Becker R. H., White R. L., Helfand D. J., 1995, ApJ, 450, 559
Bernstein G. M., 2009, ApJ, 695, 652
Blake C., Bacon D., Fluke C., Kitching T., Miller L., Power C., Wilman R., 2007, SKADS Virtual Telescope Proposal, available at http://www.skads-eu.org/p/svt/svt2007.php
Booth R. S., de Blok W. J. G., Jonas J. L., Fanaroff B., 2009, preprint (arXiv:0910.2935)
Brainerd T. G., Agustsson I., Madsen C. A., Edmonds J. A., 2009, preprint (arXiv:0904.3095)
Bridle S., King L., 2007, New J. Phys., 9, 444

Brown M. L., Taylor A. N., Hambly N. C., Dye S., 2002, MNRAS, 333, 501
Brown M. L., Castro P. G., Taylor A. N., 2005, MNRAS, 360, 1262
Burns C. R., Dyer C. C., Kronberg P. P., Röser H., 2004, ApJ, 613, 672
Catelan P., Kamionkowski M., Blandford R. D., 2001, MNRAS, 320, L7
Chang T., Refregier A., Helfand D. J., 2004, ApJ, 617, 794
Clarke J. N., Kronberg P. P., Simard-Normandin M., 1980, MNRAS, 190, 205
Crittenden R. G., Natarajan P., Pen U., Theuns T., 2001, ApJ, 559, 552
Croft R. A. C., Metzler C. A., 2000, ApJ, 545, 561
Dyer C. C., Shaver E. G., 1992, ApJ, 390, L5
Eisenstein D. J., Hu W., 1999, ApJ, 511, 5
Faraoni V., 1993, A&A, 272, 385
Fu L. et al., 2008, A&A, 479, 9
Górski K. M., Hivon E., Banday A. J., Wandelt B. D., Hansen F. K., Reinecke M., Bartelmann M., 2005, ApJ, 622, 759
Grant J., Taylor R., Stil J., Landecker T., Kothes R., Ransom R., Scott D., 2010, ApJ, 714, 1689
Heavens A., Refregier A., Heymans C., 2000, MNRAS, 319, 649
Heymans C., Heavens A., 2003, MNRAS, 339, 711
Heymans C., Brown M., Heavens A., Meisenheimer K., Taylor A., Wolf C., 2004, MNRAS, 347, 895
Heymans C., White M., Heavens A., Vale C., van Waerbeke L., 2006, MNRAS, 371, 750
Hikage C., Takada M., Hamana T., Spergel D., 2010, preprint (arXiv:1004.3542)
Hirata C. M., Seljak U., 2004, Phys. Rev. D, 70, 063526
Hirata C. M., Mandelbaum R., Ishak M., Seljak U., Nichol R., Pimbblet K. A., Ross N. P., Wake D., 2007, MNRAS, 381, 1197
Hivon E., Górski K. M., Netterfield C. B., Crill B. P., Prunet S., Hansen F., 2002, ApJ, 567, 2
Jing Y. P., 2002, MNRAS, 335, L89
Joachimi B., Bridle S. L., 2009, preprint (arXiv:0911.2454)
Joachimi B., Schneider P., 2008, A&A, 488, 829
Joachimi B., Schneider P., 2009, A&A, 507, 105
Johnston S. et al., 2008, Exp. Astron., 22, 151
Kaiser N., Wilson G., Luppino G. A., 2000, preprint (astro-ph/0003338)
King L. J., 2005, A&A, 441, 47
King L., Schneider P., 2002, A&A, 396, 411
King L. J., Schneider P., 2003, A&A, 398, 23
Kirk D., Bridle S., Schneider M., 2010, preprint (arXiv:1001.3787)
Kronberg P. P., Dyer C. C., Burbidge E. M., Junkkarinen V. T., 1991, ApJ, 367, L1
Kronberg P. P., Dyer C. C., Roeser H., 1996, ApJ, 472, 115
Mackey J., White M., Kamionkowski M., 2002, MNRAS, 332, 788
Mandelbaum R., Hirata C. M., Ishak M., Seljak U., Brinkmann J., 2006, MNRAS, 367, 611
Mandelbaum R. et al., 2009, prperint (arXiv e-prints, 0911.5347)
Massey R., Kitching T., Richard J., 2010, Rep. Progress Phys., 73, 086901
Morganti R. et al., 2010, preprint (arXiv:1001.2384)
Patel P., Bacon D. J., Beswick R. J., Muxlow T. W. B., Hoyle B., 2010, MNRAS, 401, 2572
Peacock J. A., Schneider P., Efstathiou G., Ellis J. R., Leibundgut B., Lilly S. J., Mellier Y., 2006, Tech. Rep., preprint (astro-ph/0610906)
Schneider M. D., Bridle S., 2010, MNRAS, 402, 2127
Sereno M., 2005, MNRAS, 359, L19
Smith R. E. et al., 2003, MNRAS, 341, 1311
Stil J. M., Krause M., Beck R., Taylor A. R., 2009, ApJ, 693, 1392
Subrahmanyan R., Ekers R. D., Saripalli L., Sadler E. M., 2010, MNRAS, 402, 2792
Surpi G. C., Harari D. D., 1999, ApJ, 515, 455
Takada M., White M., 2004, ApJ, 601, L1
Taylor A. R. et al., 2007, ApJ, 666, 201
Van Waerbeke L. et al., 2000, A&A, 358, 30
Wilman R. J. et al., 2008, MNRAS, 388, 1335
Wittman D. M., Tyson J. A., Kirkman D., Dell'Antonio I., Bernstein G., 2000, Nature, 405, 143
York D. G. et al., 2000, AJ, 120, 1579
Zhang P., 2010, ApJ, 720, 1090

APPENDIX A: DISPERSION OF THE NEW ESTIMATOR

If we define for each galaxy within a pixel

$$\boldsymbol{n}_i^{\parallel} = \begin{pmatrix} \cos 2\alpha_i^{\rm int} \\ \sin 2\alpha_i^{\rm int} \end{pmatrix}; \quad \boldsymbol{n}_i^{\perp} = \begin{pmatrix} \sin 2\alpha_i^{\rm int} \\ -\cos 2\alpha_i^{\rm int} \end{pmatrix}, \tag{A1}$$

then the observed ellipticities can be written as

$$\boldsymbol{\epsilon}_i^{\rm obs} = \boldsymbol{\epsilon}_i^{\rm int}\boldsymbol{n}_i^{\parallel} + \delta\boldsymbol{\epsilon}_i + \boldsymbol{\gamma}, \tag{A2}$$

where $\delta\boldsymbol{\epsilon}_i$ is the measurement error on the observed (total) ellipticity of the ith galaxy. If the combined astrophysical and measurement errors on the observed intrinsic PAs are $\delta\alpha_i$, then

$$\hat{\boldsymbol{n}}_i = \begin{pmatrix} \sin(2\alpha_i^{\rm int} + 2\delta\alpha_i) \\ -\cos(2\alpha_i^{\rm int} + 2\delta\alpha_i) \end{pmatrix} = \boldsymbol{n}_i^{\perp}\cos 2\delta\alpha_i + \boldsymbol{n}_i^{\parallel}\sin 2\delta\alpha_i. \tag{A3}$$

These can be substituted into equations (14) and (15) to give

$$\mathbf{A} = \sum_i w_i \left[\boldsymbol{n}_i^{\perp}\boldsymbol{n}_i^{\perp\rm T}\cos^2 2\delta\alpha_i + \boldsymbol{n}_i^{\parallel}\boldsymbol{n}_i^{\parallel\rm T}\sin^2 2\delta\alpha_i + \left(\boldsymbol{n}_i^{\parallel}\boldsymbol{n}_i^{\perp\rm T} + \boldsymbol{n}_i^{\perp}\boldsymbol{n}_i^{\parallel\rm T}\right)\sin 2\delta\alpha_i\cos 2\delta\alpha_i\right], \tag{A4}$$

$$\boldsymbol{b} = \mathbf{A}\boldsymbol{\gamma} + \delta\boldsymbol{\epsilon} + \delta\boldsymbol{b}, \tag{A5}$$

where

$$\delta\boldsymbol{\epsilon} = \sum_i w_i(\delta\boldsymbol{\epsilon}_i\cdot\hat{\boldsymbol{n}}_i)\hat{\boldsymbol{n}}_i, \tag{A6}$$

$$\delta\boldsymbol{b} = \sum_i w_i\boldsymbol{\epsilon}_i\sin 2\delta\alpha_i\left(\boldsymbol{n}_i^{\perp}\cos 2\delta\alpha_i + \boldsymbol{n}_i^{\parallel}\sin 2\delta\alpha_i\right). \tag{A7}$$

Hence, from equations (13) and (A5), the estimator is given by

$$\hat{\boldsymbol{\gamma}} = \boldsymbol{\gamma} + \mathbf{A}^{-1}\delta\boldsymbol{\epsilon} + \mathbf{A}^{-1}\delta\boldsymbol{b}. \tag{A8}$$

Ignoring the measurement errors on the galaxy ellipticities, $\delta\boldsymbol{\epsilon}_i = 0$, and assuming small errors on the intrinsic PAs, $\delta\alpha_i \ll 1$, to order $\delta\alpha^2$, equation (A8) can be written as

$$\hat{\boldsymbol{\gamma}} = \boldsymbol{\gamma} + 2\sum_i w_i\,\delta\alpha_i^{\rm int}\boldsymbol{\epsilon}_i\,\mathbf{A}^{-1}\boldsymbol{n}_i^{\perp} + \mathcal{O}(\delta\alpha^2), \tag{A9}$$

and the matrix, $\mathbf{A}$, is

$$\mathbf{A} = \mathbf{A}^{\perp} + \mathcal{O}(\delta\alpha) = \sum_i w_i\boldsymbol{n}_i^{\perp}\boldsymbol{n}_i^{\perp\rm T} + \mathcal{O}(\delta\alpha). \tag{A10}$$

Therefore, ignoring $\mathcal{O}(\delta\alpha^2)$, we have

$$\hat{\boldsymbol{\gamma}} - \boldsymbol{\gamma} \approx 2\sum_i w_i\,\delta\alpha_i\boldsymbol{\epsilon}_i\,(\mathbf{A}^{\perp})^{-1}\boldsymbol{n}_i^{\perp}. \tag{A11}$$

Without loss of generality, we can assume uniform weights (normalized such that $\sum_i w_i = 1$) and writing $\boldsymbol{m}_i^{\perp} = (\mathbf{A}^{\perp})^{-1}\boldsymbol{n}_i^{\perp}$, equation (A11) is

$$\hat{\boldsymbol{\gamma}} - \boldsymbol{\gamma} \approx \frac{2}{N}\sum_i \delta\alpha_i\boldsymbol{\epsilon}_i\,\boldsymbol{m}_i^{\perp}, \tag{A12}$$

where N is the number of galaxies in the pixel. If we now assume that $\delta\alpha_i$, $\boldsymbol{\epsilon}_i$ and $\boldsymbol{m}_i^{\perp}$ are independent, then we have

$$\hat{\boldsymbol{\gamma}} - \boldsymbol{\gamma} \approx 2\left(\frac{1}{N}\sum_i\delta\alpha_i\right)\left(\frac{1}{N}\sum_i\boldsymbol{\epsilon}_i\right)\left(\frac{1}{N}\sum_i\boldsymbol{m}_i^{\perp}\right). \tag{A13}$$

Taking the limit as $N \to \infty$, in the absence of an IA signal, $\langle \boldsymbol{m}^{\perp} \rangle = \langle \boldsymbol{\epsilon} \rangle = 0$, and assuming the intrinsic PA estimates are unbiased, $\langle \delta\alpha^{\rm int} \rangle = 0$. Thus, we have $\langle \hat{\boldsymbol{\gamma}} \rangle = \boldsymbol{\gamma}$ as required. For N finite, the standard error will be given by

$$\sigma_{\hat{\boldsymbol{\gamma}}} \approx 2 \frac{\langle \delta\alpha^2 \rangle^{1/2} \langle \boldsymbol{\epsilon}^2 \rangle^{1/2} \langle \boldsymbol{m}^{\perp 2} \rangle^{1/2}}{\sqrt{N}}. \tag{A14}$$

For randomly distributed true PAs, we find that $\langle \boldsymbol{m}^{\perp 2} \rangle = 4$. Thus, the error in the estimator is

$$\sigma_{\hat{\boldsymbol{\gamma}}} \approx 4 \frac{\alpha_{\rm rms}\, \boldsymbol{\epsilon}_{\rm rms}}{\sqrt{N}}. \tag{A15}$$

This paper has been typeset from a TEX/LATEX file prepared by the author.